

**Fermi National Accelerator Laboratory**

**FERMILAB-Pub-87/141**

## **Elastic Scattering in Thick Targets and Edge Scattering\***

A. Van Ginneken  
Fermi National Accelerator Laboratory  
P.O. Box 500, Batavia, Illinois 60510

September 1987

\*To be submitted for journal publication



**Operated by Universities Research Association Inc. under contract with the United States Department of Energy**

# Elastic Scattering in Thick Targets and Edge Scattering

A. Van Ginneken

Fermi National Accelerator Laboratory\*  
P. O. Box 500, Batavia, IL 60510

September 1987

## Abstract

Physical processes causing limited ( $< \sim 1\%$ ) energy loss to high energy particles traversing bulk matter are examined and their cross sections cast in a form suitable for use in Monte Carlo transport calculations. Special attention is paid to scattering off edges. An algorithm is developed, based on the Fermi distribution of multiple Coulomb scattering, which generates first passage distributions for escaping particles and more generally for transport of particles undergoing multiple scattering in the presence of an edge. Implementation of the various processes and of the edge scattering algorithm into a Monte Carlo code are briefly indicated. A sample of results obtained with this code is included.

## 1 Introduction

For a variety of problems encountered in particle transport in bulk matter, interest is restricted to particles with energies very near to the incident energy, i.e., those identifiable as incident particles and which only participated in elastic or quasi-elastic processes. Around high energy accelerators such problems arise when beam particles interact with the beampipe, scrapers, septa, etc., often with undesired consequences. To address such questions

---

\*Fermi National Accelerator Laboratory is operated by Universities Research Association under contract with the US Department of Energy.

a Monte Carlo (MC) code, referred to as ELSIM, owes its existence. This paper presents the physical models and approximations on which this code is based. Where appropriate, MC procedures are indicated.

In accelerator related problems, one reason for concentrating on particles close in energy to the beam is because these particles may travel with the beam for considerable distances, thereby creating a set of problems which can be properly analyzed only by starting out from a reasonably detailed description of the phase space occupied by these particles. Particles differing in energy substantially from the beam create other problems which typically have very little overlap with the elastic type and are analyzed by different means [1]. The present code may have to be supplemented by other codes for comprehensive studies, e.g., at Fermilab problems of radiation induced quenching during resonant extraction have been examined [2] using a three-code combination: (a forerunner of) ELSIM to study elastic processes, a code which tracks the elastics magnet-by-magnet through the accelerator lattice and the MC code CASIM [1] to calculate energy deposition wherever the elastics intercept the beampipe and begin to initiate hadronic and electromagnetic showers.

The physical processes included are: (1) multiple Coulomb scattering (mCs), (2) coherent and incoherent nuclear elastic scattering, (3) single diffractive excitation of a target nucleon, (4) energy loss by collision with atomic electrons ( $dE/dx$ ), but treating separately (5) encounters with large momentum transfer, (6) bremsstrahlung, (7) direct pair production. The last three processes will occasionally lead to a large energy loss ( $>\sim 1\%$ ) and hence removal of the particle from the elastic set. The latter always occurs for (8) nuclear absorption. Of these processes (1) and (4) are assumed to take place continuously along the track of the particle, while all others are treated as discrete events taking place at a point. Item (2) includes large angle Coulomb scattering as well as its interference with nuclear scattering and is thus not mutually exclusive with (1), making a more precise delineation necessary. This is also the case for items (4) and (5) as well as (3) and (8). These and other matters regarding the physical processes are discussed in sec. 2.

A type of problem connected with elastic processes, which arises in practical applications, concerns the fate of a particle inside a thick target but close to the surface and nearly parallel to it as occurs, e.g., when a particle strikes the surface at a very shallow angle and has a significant chance to be reflected back out of the target. Simulation of mCs by applying a finite deflection at finite intervals becomes invalid when the escape probability

within an interval and hence precise particle position and direction at escape, are poorly monitored. Reducing the step size sufficiently to overcome this can easily become too consumptive of computer time. Beam collimation as well as accidental scraping pose problems of this type. An algorithm to study such problems is introduced in sec. 3.

From the point of view of applications the most important projectiles are protons ( $p$  as well as  $\bar{p}$ ) and electrons. The ELSIM code is specifically written for proton projectiles and results presented here are limited to protons. Sec. 4 contains a sampling of results obtained with the code. Extension to other hadrons requires minimal alteration. For electrons and muons the relevant physical processes are a subset of the ones enumerated above. Although there is considerable shift in emphases among the processes, as well as in distance scales, adaptation to the lepton projectiles appears straightforward. Adaptation to a simple magnetic environment such as a uniform magnetic field should not pose any difficulties although synchrotron radiation may have to be included, especially for electrons.

The valid momentum range of this code is roughly from 1 GeV/c to 30 TeV/c. Above this range the parametrizations of bremsstrahlung and pair production used in the code remain unchecked against more detailed *ab initio* calculations. Below  $\sim 1$  GeV/c the nuclear scattering model is not well validated. The assumption of a constant rms angle for mCs (at least within one step) as well as the small angle approximation, which permeates most scattering algorithms employed here, preclude application at significantly lower energies.

## 2 Physical Processes

The different physical processes included in the program, i.e., those enumerated above, are discussed in this section along with some indication of the MC implementation, where appropriate.

### 2.1 Multiple Coulomb Scattering

The treatment of small angle mCs used here is based on the Fermi distribution of multiple scattering (sec. 3), which predicts a Gaussian angular distribution (in projected angle) for a beam of particles traversing a fixed target thickness. A well known criticism of this approximation is that, for not so thick targets, it fails badly at large angles where single scattering ‘tails’

dominate the Gaussian [3]. This criticism is circumvented by adopting a judiciously chosen cut-off angle,  $\theta_0$ , below which the scattering is treated in the Gaussian approximation and above which it is treated event-by-event using predictions of Glauber [4,5]. The determination of  $\theta_0$  is sketched below.

For a Coulomb potential,  $Ze/r$ , cut off at the atomic radius, the Rutherford scattering cross section for a particle of unit charge, momentum,  $p$ , and velocity,  $v$ , may be written as

$$d\sigma/d\Omega = (2Ze^2/pv)^2/(\theta^2 + \theta_{min}^2)^2 \quad (1)$$

where

$$\theta_{min} \simeq Z^{1/3}m_e c/Kp. \quad (2)$$

Usually  $K \simeq 200$  is assumed, where  $K$  is dimensionless. Here, instead of being a constant,  $K$  is allowed to vary with  $Z$ , with its dependence determined from experiment. Nevertheless,  $K$  retains this order of magnitude. An advantage of eq. 1 over more sophisticated treatments is that it yields a simple expression for the rms angle of scattering through a foil of thickness  $t$ , containing  $N$  atoms per unit volume:

$$\langle \theta^2 \rangle = \pi N t (2Ze^2/pv)^2 \left\{ \ln \left[ (\theta_0/\theta_{min})^2 + 1 \right] - 1 \right\}. \quad (3)$$

Usually  $\theta_0$  is identified with  $\theta_{max}$  where  $\theta_{max}$  is obtained from considerations of nuclear size. Here  $\theta_0 = \delta\theta_{max}$  with  $\delta < 1$  is assumed. In addition,  $\delta$  is chosen such that  $\theta_0^2$  is at most of order  $\langle \theta^2 \rangle$  where  $\langle \theta^2 \rangle$  is proportional to step size as in eq. 3. This second constraint on  $\delta$  ensures that single scattering angles  $\leq \theta_0$  are well confined within the mCs Gaussian, which in turn helps justify the Gaussian approximation.

A most practical choice of step size is the (randomly varying) distance between large angle scatterings (including absorption) with as its average  $\lambda = 1/N\sigma_{tot}$ , where  $\sigma_{tot}$  is the total cross section summed over all ‘point’ processes listed in sec. 1. For  $\delta \ll 1$ , the dominant contribution to  $\sigma_{tot}$  comes from Coulomb scattering with  $\theta > \theta_0$ , so that  $\sigma_{Coul}$  may be used to find a suitable  $\delta$ . Integrating eq. 1 between  $\theta_0$  and infinity yields:

$$\sigma_{Coul} \simeq \sigma_{tot} \simeq \pi(2Ze^2/pv)^2/\theta_0^2. \quad (4)$$

For  $\theta_0 = \delta\theta_{max} = \delta 274(m_e c/p)A^{-1/3}$  this may be rewritten as

$$\sigma_{Coul} \simeq 0.0133Z^2 A^{2/3}/\delta^2 \quad mb. \quad (5)$$

If  $\delta$  is chosen to be proportional to  $Z$ , i.e.,  $\delta = \beta Z$ , then from eq. 5

$$\lambda_{Coul} \simeq \lambda \simeq 1.25 \cdot 10^5 A^{1/3} \beta^2 \quad g/cm^2 \quad (6)$$

while the ratio  $\langle \theta^2 \rangle / \theta_0^2$  becomes

$$\langle \theta^2 \rangle / \theta_0^2 \simeq 2 \ln(4.2 \cdot 10^4 \beta Z^{1/3}) \quad (7)$$

where  $A \simeq 2Z$  and  $K = 192$  are used. For a value of  $\beta \simeq 3 \cdot 10^{-3}$  both inequalities  $\delta < 1$  (since  $Z < \sim 100$ ) and  $\langle \theta^2 \rangle / \theta_0^2 > 1$  (see eq. 7, since  $Z \geq 1$ ) hold while  $\lambda \simeq 1.1 A^{1/3}$  in  $g/cm^2$  is generally quite suitable as a step length in terms of target dimensions and computer time economy.

The value of  $K$  in eq. 2 is now allowed to vary with  $Z$  and is determined from the experimental results of Shen et al. [7] which measured  $\langle \theta^2 \rangle$  for thin targets of various  $Z$  in the 50–200 GeV/c momentum range using p,  $\pi$  and K projectiles. In this experiment  $\langle \theta^2 \rangle$  is found to have the expected  $p^{-2}$  behavior and to be independent of projectile type. Shen et al. fit their data to the three parameter function:

$$d\sigma/d\Omega = exp \left[ A - (1 + C)(\theta/\theta_e)^2 + C(\theta/\theta_e)^4 \right] \quad (8)$$

which approximates the Molière distribution [6].

To fix  $K(Z)$ , and hence  $\theta_{min}$ , for a given  $Z$  a MC simulation of repeated single elastic scattering based on Glauber's theory (see below) is performed for individual scattering angles above  $\theta_0$  and for target thicknesses roughly as in the experiment of Shen et al. [7]. The effect of angles  $< \theta_0$  is introduced by combining the results with a set of random angles drawn from Gaussian distributions with  $\sigma$ 's, or equivalently  $K(Z)$ 's, corresponding to different  $\theta_{min}$ . The resulting distributions are then fitted to eq. 8. The effect of the uncertainty in  $\theta_e$  in this parametrization is studied by varying  $\theta_e$  ( $C$  is fixed by Shen et al. at its Molière predicted value). Fig. 1 shows  $K(Z, \theta_e)$  as a function of  $Z$  along with  $K(Z, \theta_e \pm \sigma_{\theta_e})$  as indicated by the error bars. The values used in ELSIM of  $K(Z)$  are obtained from a least squares fit through  $K(Z, \theta_e)$ :

$$K(Z) = 837 Z^{-0.54}. \quad (9)$$

The  $\chi^2$  of the above fit is sensitive to the choice of  $\theta_0$  but  $K(Z)$  is only marginally affected. The fit of  $K$  (and  $\theta_{min}$ ) to experiment justifies the use of eq. 1 to determine  $\langle \theta^2 \rangle$  in lieu of more sophisticated treatments, e.g. ref. [6].

The dichotomy of the problem into single and multiple scattering regimes remains, of course, an approximation. There exists some angular regime where ‘plural’ scattering dominates, but which here is folded into the mCs Gaussian. The choice of a cut-off angle in the above manner ensures that the approximation is reasonable for sufficiently large step sizes. A related assumption is that mCs takes place continuously along the particle’s track which obviously must fail at small enough distances.

## 2.2 Nuclear Scattering

For the present purpose nuclear scattering includes large angle Coulomb scattering plus coherent nuclear scattering and their interference as well as incoherent nuclear scattering. For hadron projectiles this forms, along with mCs, the most important ingredient of the calculation. The treatment adopted here is that of Glauber [4,5]. The energy dependent parameters of p-p scattering are taken from experiment [8]. For simplicity the p-neutron hadronic scattering parameters are assumed to match those of p-p. The nuclear density model used by Glauber is the harmonic oscillator potential well for light nuclei ( $4 \leq A \leq 12$ ) and the Wood-Saxon distribution for heavier nuclei. Besides the density model, the theory is formulated differently for light and heavy nuclei. For the latter, the assumption that the range of nuclear forces is much smaller than the nuclear radius results in significant simplification. However, even for beryllium and carbon the heavy nucleus prescription is still quite accurate [5]. For convenience then, the heavy nucleus formulation of the theory (but with harmonic oscillator densities for light nuclei) is adopted throughout.

Extensive comparisons with experiment (below 20 GeV) are reported in ref. [5]. Agreement with the 19.3 GeV/c proton data of Belletini et al. [9], among others, is excellent for reasonable values of the nuclear parameters. The comparison is extended here to the 70–175 GeV/c range, where measurements for a variety of nuclear species and incident hadrons are reported by Schiz et al. [10]. Figs. 2 and 3 illustrate the fits for a representative sample of the proton data. In addition to Coulomb and nuclear scattering, the graphs include a relatively small component from particle producing processes (see sec. 2.3 below) as indicated in the figures.

The nuclear parameters are derived from electron scattering [11], where necessary by interpolation. No attempt is made at adjusting the parameters to improve the fit, which is also not very sensitive to this, e.g., changing the parameters to those preferred by Glauber and Matthiae [5] yields a fit only

slightly inferior to that of figs. 2 and 3. Along with parameter adjustments and more detailed treatment of the light nuclei, a number of other improvements to the calculation could well result in a better fit, e.g. , more accurate representation of p-p and especially p-n scattering, separate calculations for each isotope present instead of using a single set of averaged nuclear properties, inclusion of elastic and diffractive interaction with nuclear fragments, etc. However, as can be seen from the figures, Glauber theory with this choice of parameters fits the data quite well over a region of momentum transfer which includes essentially all of the coherent and most of the incoherent cross section. With the proper energy dependence of the hadron-p and h-n scattering parameters, the model should apply equally well to other hadrons and at other energies.

In the MC program Coulomb and coherent nuclear scattering are combined but treated separately from incoherent scattering. Sampling of scattering angles is performed via detailed look-up tables calculated from Glauber theory, since the cross sections are in the form of rather complicated multiple integrals making direct sampling impractical.

### 2.3 Diffractive Target Dissociation

In the MC simulation, an inelastic interaction with a target nucleus typically removes the particle from further consideration (see sec. 2.6). Exception is made for single diffractive events where the *target* particle is excited to a low mass state, which implies (typically) that the projectile continues with only slight changes in energy and direction. The minimum energy loss of the projectile in such events is of order of the pion mass which, in the regime of interest here, is always a small fraction of the projectile's energy. Below, the term single diffraction refers to this type of event only. Diffractive excitation of the projectile and subsequent decay usually incurs much larger energy losses by the projectile particle and is therefore not of interest here.

The description of p-p diffractive processes is adapted from the review of Goulianos [12]:

$$\begin{aligned} d\sigma/dtdM^2 &= 0.6b_D(1 + 36/s) \frac{M^2 - M_p^2}{1 + M_p^2} e^{b_D t} \quad M^2 \leq 1 + M_p^2 \\ &= 0.6b_D(1 + 36/s) \exp(b_D t)/M^2 \quad M^2 \geq 1 + M_p^2 \end{aligned} \quad (10)$$

where  $M_p^2$ ,  $M^2$ ,  $s$  denote the square of the invariant mass resp. , of the proton, of the diffractively produced state and of the entire collision;  $t$  is the square

of the 4-momentum transfer and  $b_D$  depends on  $M^2$  via the following simple parametrization based on experiment (see also ref. [12]):

$$\begin{aligned} b_D &= 2b_{el} & M^2 \leq 1 + M_p^2 \\ &= [2b_{el} - 8(M^2 - M_p^2 - 1), 7]_{max} & M^2 \geq 1 + M_p^2 \end{aligned} \quad (11)$$

where  $b_{el}$  is the slope parameter for elastic scattering at low  $t$ . In both of the above expressions masses, etc., are expressed in  $GeV$ ,  $b_{el}$  is in  $GeV^{-2}$  and the cross section of eq. 10 is in  $mb \cdot GeV^{-4}$ . Eq. 10, integrated up to a limit [12] of  $M^2 = s/10$  yields a total cross section for single diffraction (in  $mb$ ):

$$\sigma_{sd} = 0.6(1 + 36/s) \left[ 1/2(1 + M_p^2) + \ln(0.1s/1 + M_p^2) \right]. \quad (12)$$

The above parametrizations are based on experiments which observe target excitation in the lab frame using incident protons in the 100–400  $GeV/c$  range. It also describes ISR [13] and CERN Collider [14] results reasonably well provided experimental momentum resolutions are folded into the comparison.

The expressions for p-nucleon single diffraction may be applied to a nuclear target in the usual approximation that the particle traverses the nucleus in a straight line and, at a given impact parameter,  $\vec{b}$ , encounters an average number of nucleons  $T(b) = \int_{-\infty}^{\infty} \rho(\hat{k}z + \vec{b}) dz$  per unit area. The nuclear density parameters are those adopted for elastic scattering (sec. 2.2). If a single nucleon encounter is classified as either elastic, single diffractive or absorptive, then the only composite diffractive events of interest here are those with one or more diffractive nucleon encounters plus any number of elastics but no absorption. The total cross section for ‘compound single’ diffraction off a nucleus is therefore

$$\sigma_{sd}^A = \int_0^{\infty} (1 - e^{-T(b)\sigma_{sd}}) e^{-T(b)\sigma_{abs}} 2\pi b db \quad (13)$$

where  $\sigma_{abs} = \sigma_{tot} - \sigma_{el} - \sigma_{sd}$ . For convenience diffractive p-neutron scattering is assumed identical to p-p scattering though there are substantial differences [15], at least for  $p_x/p_z^{max}$  below 0.9. Fig. 4 shows  $\sigma_{sd}$  from eq. 12 for p-p, as well as  $\sigma_{sd}^A$  from eq. 13 for protons on selected nuclear targets, as a function of momentum.

The addition of a nuclear single diffractive component, calculated in this fashion, to the elastic  $d\sigma/dt$  is shown in figs. 2 and 3. This is not necessarily meant to improve the comparisons, though it may well succeed therein

in some instances. Since the experiment [10] exercises a (necessarily incomplete) veto on inelastic events this may suppress some single diffractive events, especially at large  $t$ . The presence of this component in the comparisons is mainly to indicate its relative importance and to demonstrate that its presence does not contradict experiment.

The  $\sigma_{sd}^A$  provide a measure of the fraction of  $\sigma_{tot}$  leading to events of this type. This process is fully included in the MC calculation with the nuclear inelastic cross sections lowered accordingly. When such an event is encountered in the MC simulation, an impact parameter, or equivalently an average number of nucleon encounters per unit area, is selected from  $\sigma^{-1}d\sigma/db$ , where  $d\sigma/db$  is essentially the integrand of eq. 13. To represent fluctuations about this average, a random number of encounters,  $n_r$ , is selected from a truncated Poisson distribution, i.e., with  $n_r = 0$  and  $n_r > A$  excluded. Simulation of the nuclear event is then replaced by successively simulating a chain of  $n_r$  diffractive and elastic events. Since there must be at least one diffractive encounter, and since the order within the chain has little or no effect on the final outcome, it is convenient to start with a diffractive event and assign the type of any subsequent events randomly, with probabilities proportional to  $\sigma_{el}$  and  $\sigma_{sd}$ .

## 2.4 Energy Loss by Collision

Energy loss by collision with atomic electrons is divided into small energy losses (the so-called restricted  $dE/dx$ ) assumed to take place continuously along the track of the particle, and large energy transfers which are treated as point processes. The restricted  $dE/dx$ , which approaches a limiting value as opposed to increasing logarithmically with energy, is calculated using the familiar Bethe-Bloch formula with Sternheimer corrections [16], but with the kinematic limit of energy transfer per collision replaced by a somewhat arbitrary cut-off energy, set here at  $\Delta E = 10$  MeV. Much lower  $\Delta E$  lead to excessive sampling of ‘large’ energy transfer events. Much higher  $\Delta E$  will seriously underestimate fluctuations in  $dE/dx$  of the particle.

For large energy transfer to atomic electrons the cross section is basically that of Rutherford scattering but transformed from  $d\sigma/d\Omega$  to  $d\sigma/dT_e$  where  $T_e$  is the kinetic energy acquired by the electron (assumed to be unbound). It is readily adapted for MC sampling. The angular deflection of the projectile,  $\theta$ , is related to  $T_e$ , which is proportional to the 4-momentum transfer of the collision

$$-t = 2m_e T_e \simeq p^2 \theta^2 \quad (14)$$

where  $p$  is the projectile momentum. For  $T_e = 10$  MeV,  $\theta$  is of the order of  $\theta_0$  from sec. 2.1, above which Coulomb scattering is treated on an individual event basis, so that both treatments are consistent in this respect.

## 2.5 Bremsstrahlung and Direct Pair Production

The energy loss and angular deflection associated with bremsstrahlung and pair production are simulated in the manner outlined in ref. [17]. Both are important in the TeV regime, although for the present application they may well be negligible in many cases. The basic algorithm consists of selecting the fractional energy loss of the fast particle,  $v$ , from a parametrization devised expressly for convenience in MC sampling which approximates numerical results obtained from detailed *ab initio* calculations of  $\sigma^{-1}d\sigma/dv$ . (If  $v$  exceeds some preset  $v_0$  ( $\sim 1\%$ ), the event is considered equivalent to absorption for the present purpose.) Next, the rms angle of the fast particle,  $\langle\theta^2\rangle^{1/2}$ , which depends on  $v$ , is obtained from a simple formula, likewise based on more detailed calculations. A random angle is then selected from a Gaussian with  $\sigma = \langle\theta^2\rangle^{1/2}$  to complete the event simulation.

The criticism leveled at the Gaussian approximation of the mCs [3] applies here as well. Specific inclusion of the ‘tails’, e.g., by a split as in sec. 2.1, would be a definite improvement. However, for applications of the type addressed here (see sec. 1) the particles belonging to these tails are likely to be of lesser interest.

## 2.6 Nuclear Absorption

An inelastic interaction (i.e. accompanied by particle production), with the exception of single diffraction (see sec. 2.3) essentially means removal of the particle from the elastics in the MC. When necessary, initial coordinates, etc., are recorded as input for other calculations. For problems connected with deep penetration one might alternatively treat nuclear absorption as continuously taking place along the track, in lieu of as a point process. This is accomplished by attaching to the particles a weight of  $\exp(-z/\lambda_{abs})$ , where  $z$  is measured essentially along the incident particle direction.

## 3 Edge Scattering

This section describes an algorithmic approach to mCs in the presence of an edge. An ‘edge problem’ exists only for mCs and is tied to the approx-

imation that the angle varies continuously along the track of the particle. For point processes (or continuous processes which do not affect the particle's direction) the MC treatment is essentially analog and the geometry, including any edges, can be modelled to arbitrary accuracy. In this context it should be remarked that geometrical imperfections may well bear on the problem and that these may be difficult to analyze and to represent, e.g., the 'flat' edge of a beam scraper is neither a plane nor does it likely even resemble a regular surface when examined in sufficient detail. The dichotomy into single and multiple scattering is also related to this. These difficulties are not further addressed here but they should nonetheless be kept in mind when interpreting results.

The basic flow of the MC calculation transports the particle from its point of incidence, through a number ( $\geq 0$ ) of elastic interactions, each of which changes the direction and energy of the particle (see sec. 2), to eventual absorption or escape. Following each interaction (as well as at the point of incidence) escape from an infinitely long target, i.e., the *first passage*, is simulated. The distance to escape is then compared with the randomly selected distance to the next discrete event (as in a homogeneous target) or, in a target of finite length, with back escape. The problem is therefore to devise MC schemes to simulate the first passage as well as to find the location of the successive points of interaction (or escape), and the particle's direction at each point, taking into account mCs and the presence of an edge.

The method proposed is reminiscent of Kelvin's method of images which has already served a similar purpose in 'ballot theorems' [18] and first passage times in Brownian motion [19]. The problem of mCs in a *block* of finite or infinite length is the only application considered here. But the approach is quite general and is not limited to mCs, flat surfaces or the small angle approximation.

The remainder of this section discusses first the Fermi distribution which describes mCs in a homogeneous target and sets the stage for the introduction of the edge scattering algorithms, which vary somewhat in character depending on the geometry: edge-to-edge, front-to-edge and front (or edge)-to-back.

### 3.1 Homogeneous Target

For mCs in a homogeneous target the Fermi distribution [20] applies. In full generality:

$$F(\mathbf{x}, \mathbf{x}' | \mathbf{x}_0, \mathbf{x}'_0, z) = (2\sqrt{3}/\pi\theta_s^2 z^2) \cdot e^{-(4/\theta_s^2 z)[(\mathbf{x}' - \mathbf{x}'_0)^2 - 3(\mathbf{x}' - \mathbf{x}'_0)(\mathbf{x}/z - \mathbf{x}_0/z - \mathbf{x}'_0) + 3(\mathbf{x}/z - \mathbf{x}_0/z - \mathbf{x}'_0)^2]} \quad (15)$$

where  $|$  in  $F(\cdot | \cdot)$  separates the given parameters  $\mathbf{x}_0, \mathbf{x}'_0, z$  from the variables  $\mathbf{x}, \mathbf{x}'$  (initially  $\mathbf{x}_0, \mathbf{x}'_0$ ) which denote respectively the lateral displacement and its derivative with respect to  $z$ , the distance in the  $\mathbf{x}'_0 = 0$  direction;  $\theta_s$  is the rms (spatial) angle per unit length (see sec. 2.1). There is an entirely similar distribution for  $y, y'$ . The origin of this formula is attributed to Fermi [20]. It was rederived by Eyges [21] and by Scott [22] by formulating and solving a second order partial differential equation. An alternative derivation of eq. 15 follows from probability arguments and is sketched heuristically in app. A.

Eq. 15, integrated over all  $\mathbf{x}'$ , yields a Gaussian

$$F(\mathbf{x} | \mathbf{x}_0, \mathbf{x}'_0, z) = (\sqrt{3}/\sqrt{\pi}\theta_s z^{3/2}) e^{-3(\mathbf{x} - \mathbf{x}_0 - \mathbf{x}'_0 z)^2 / \theta_s^2 z^3} \quad (16)$$

with  $\bar{\mathbf{x}} = \mathbf{x}_0 + \mathbf{x}'_0 z$  and  $\sigma = \theta_s z^{3/2} / \sqrt{6}$ . The distribution of  $\mathbf{x}'$ , for a given  $\mathbf{x}$ , is likewise Gaussian:

$$F(\mathbf{x}' | \mathbf{x}, \mathbf{x}_0, \mathbf{x}'_0, z) = (2/\sqrt{\pi}\theta_s z^{1/2}) e^{-4[\mathbf{x}' - 3(\mathbf{x} - \mathbf{x}_0)/2z + \mathbf{x}'_0/2]^2 / \theta_s^2 z} \quad (17)$$

with  $\bar{\mathbf{x}}' = 3(\mathbf{x} - \mathbf{x}_0)/2z - \mathbf{x}'_0/2$  and  $\sigma = \theta_s z^{1/2} / 2\sqrt{2}$ . This ensures fast and readily available MC schemes for sampling from eq. 15.

### 3.2 Edge-to-Edge Scattering

Eq. 15 applies to an infinitely wide block. An obvious problem arises in the presence of an edge:  $F(\mathbf{x}, \mathbf{x}' | \mathbf{x}_0, \mathbf{x}'_0, z)$  is radically altered not only in the void but also within the material since a trajectory once it crosses the edge cannot return. Therefore, predictions from eq. 15, which includes contributions of returning trajectories, overestimate the flux within the target. This is schematically displayed in fig. 5 which also shows the conventions adhered to here: the material-void boundary lies along the  $z$ -axis with the material filling the  $x > 0$  part, while the particle starts at  $z = 0$  and travels in the positive  $z$ -direction.

A convenient starting point is the problem of a beam entering and exiting the side of an infinitely long ( $-\infty < z < \infty$ ), semi-infinitely wide ( $0 < x < \infty$ ,  $-\infty < y < \infty$ ) block, as shown in fig. 6. One seeks the first passage distribution in  $z$  of the particles through the plane of the edge as well as the distribution in  $x'$  of the particles leaving the block at a given  $z$ . (Below, the joint distribution of  $z$  and  $x'$  is also referred to as a first passage distribution). The block is assumed to be infinitely wide in both  $y$ -directions hence the  $y, y'$  distribution, at any  $z$  up to the point of escape, is unaffected by the edge and follows eq. 15 [23].

The solution to the first passage problem offered here is in the form of an infinite series of convolution integrals. The series has good (exponential) convergence properties and, along with each of its individual terms, is easy to sample from in a MC calculation. No extra assumptions are invoked in its derivation, hence its level of approximation is the same as the underlying Fermi distribution: small angles, large number of scatterings, etc.

Consider (the projection onto the  $x, z$  plane of) the trajectory of a particle undergoing mCs in an infinite, homogeneous target and suppress, for the moment, all other processes. Whenever the trajectory crosses a given plane (an imaginary edge at constant  $x$ ) an index is attached to the trajectory which enumerates the crossings (see fig. 7). The total crossings (summed over all indices) for a particle starting at  $z = 0$  and at an angle  $x'_0$  with the  $z$ -axis, as a function of  $z$  and  $x'$ , is a slightly altered Fermi distribution

$$\begin{aligned} C(x', z | x_0 = 0, x'_0, x = 0) &= (2\sqrt{3}|x'|/\pi\theta_s^2 z^2) e^{-(4/\theta_s^2 z)(x'^2 + x'x'_0 + x_0'^2)} \\ &= \sum_{j=1}^{\infty} C_j(x', z) \end{aligned} \quad (18)$$

which is considerably simplified from eq. 15 by placing the edge along the  $z$ -axis but is otherwise unchanged except for the factor  $|x'|$  representing the Jacobian of the change of variables from  $x$  to  $z$ . The second equality of eq. 18 expresses  $C(x', z | 0, x'_0, 0)$  as the summation over all crossings, with  $C_j$  being the  $x', z$  distribution for the  $j^{\text{th}}$  crossing. The desired first passage distribution is then  $C_1(x', z)$ .

Eq. 18 may be decomposed into its *odd* and *even* components

$$C_o = C_1 + C_3 + \dots = (2\sqrt{3}|x'|/\pi\theta_s^2 z^2) e^{-(4/\theta_s^2 z)(x'^2 - |x'|x'_0 + x_0'^2)} \quad (19)$$

$$C_e = C_2 + C_4 + \dots = (2\sqrt{3}|x'|/\pi\theta_s^2 z^2) e^{-(4/\theta_s^2 z)(x'^2 + |x'|x'_0 + x_0'^2)} \quad (20)$$

where the arguments of the  $C_i$  are suppressed for brevity.  $C_o$  is geometrically related to  $C_e$  and  $C_1$  by a convolution over  $z_i$  combined with an integration

over  $x'_i$ :

$$C_e = C_o \star C_1 = \int_0^z \int_0^\infty C_o(x'_i, z_i | 0, x_0, 0) C_1(x', z - z_i | 0, x'_i, 0) d|x'_i| dz_i \quad (21)$$

where  $x'_i, z_i$  are the variables at the intermediate crossing and  $\star$  is shorthand for the combined convolution and integration. It follows likewise that

$$C_o - C_1 = C_e \star C_1, \quad (22)$$

which along with eq. 21 yields

$$C_1 = (C_o - C_e) + (C_o - C_e) \star C_1 \quad (23)$$

and upon iteration becomes the series

$$C_1 = (C_o - C_e) + (C_o - C_e) \star (C_o - C_e) + (C_o - C_e)^{\star 3} + \dots \quad (24)$$

with the exponential notation signifying repeated  $\star$  operations.

The first term of eq. 24, i.e., eq. 19 minus eq. 20, integrated over  $x'$

$$\int_0^\infty (C_o - C_e) d|x'| = (\sqrt{3}x'_0/2\sqrt{\pi}\theta_s z^{3/2}) e^{-3x'_0{}^2/\theta_s^2 z} \quad (25)$$

becomes a *stable distribution of index 1/2* in  $z$ . Further integration of eq. 25 over all  $z$  gives the total contribution of the  $(C_o - C_e)$  term to  $C_1$  and is equal to *one half*, which could be inferred intuitively as the fraction of all particles with  $x < 0$  at infinity. It follows that the double integral over the second term of eq. 24

$$\int_0^\infty \int_0^\infty (C_o - C_e) \star (C_o - C_e) dz d|x'| = 1/4 \quad (26)$$

and that the RHS of eq. 24 integrated term by term yields the familiar series

$$\frac{1}{2} + \frac{1}{4} + \frac{1}{8} + \dots = 1 \quad (27)$$

where the summation to unity confirms the intuitive notion that a particle entering a semi-infinite block must eventually (in the absence of absorption, etc.) emerge [24].

The series of eq. 24 is readily implemented into a fast and simple MC procedure to generate a first passage distribution in  $z, x'$  for a semi-infinite block. First, a particular term is selected from eq. 24 by comparing a uniform random number ( $0 < r < 1$ ) with the partial sums of eq. 27, i.e.,

1/2, 3/4, 7/8, ... . If the *first term* is selected ( $r < 1/2$ ) a  $z$  value is chosen from the normalized eq. 25, which is equivalent to a Gaussian distribution in  $z^{-1/2}$ . The conditional distribution of  $x'$  for given  $z$  can be written as

$$C(x'|0, x'_0, 0, z) = (\theta_s \sqrt{z} / \sqrt{\pi x'_0}) e^{x_0'^2 / \theta_s^2 z} \cdot (4|x'|/\theta_s^2 z) e^{-2x'^2 / \theta_s^2 z} \left[ e^{-2(|x'|-x'_0)^2 / \theta_s^2 z} - e^{-2(|x'+x'_0|)^2 / \theta_s^2 z} \right] \quad (28)$$

i.e., as a product of an exponential in  $x'^2$ , which is easy to sample, and the difference of two Gaussians, which can be accounted for by rejection. (This procedure is modified in unessential ways when  $x'_0$  becomes either very small or very large so as to avoid unacceptably high rejection rates.)

If, instead of the first, the  $n^{\text{th}}$  term of eq. 24 is initially selected ( $1 - 1/2^{n-1} < r < 1 - 1/2^n$ ) a chain of  $n$  ( $z_i, x'_i$ ) is produced, i.e., from  $z_0, x'_0$  a  $z_1, x'_1$  is generated in the above manner, in turn a  $z_2, x'_2$  is generated from  $z_1, x'_1$ , etc., until  $z_n, x'_n$  is obtained. A sample produced according to this algorithm is an unbiased first passage distribution in  $z, x'$  for particles with initial state  $z_0, x'_0$ .

### 3.3 Front-to-Edge Scattering

The first passage distribution for a particle entering the front and exiting the side (see fig. 5b) of a semi-infinitely long ( $0 < z < \infty$ ), semi-infinitely wide ( $0 < x < \infty, -\infty < y < \infty$ ) block is obtained in similar fashion to the edge-to-edge case. Analogous to eqs. 19 and 20:

$$D_o(x', z|x_0, x'_0, x=0) = (2\sqrt{3}|x'|/\pi\theta_s^2 z^2) \cdot e^{-(4/\theta_s^2 z)[x'^2+x_0'^2+3x'_0 x_0/z+3x_0^2/z^2-|x'|(|x'_0+3x_0/z|)]} \quad (29)$$

$$D_e(x', z|x_0, x'_0, x=0) = (2\sqrt{3}|x'|/\pi\theta_s^2 z^2) \cdot e^{-(4/\theta_s^2 z)[x'^2+x_0'^2+3x'_0 x_0/z+3x_0^2/z^2+|x'|(|x'_0+3x_0/z|)]} \quad (30)$$

where different symbols  $D_o, D_e$  ( $\neq C_o, C_e$ ) are used to indicate the different initial condition ( $x_0 \neq 0$ ). A derivation analogous to the one leading to eq. 24 results in

$$D_1 = (D_o - D_e) + (D_o - D_e) \star (C_o - C_e) + (D_o - D_e) \star (C_o - C_e)^{\star 2} + \dots \quad (31)$$

$$D_1 = (D_o - D_e) + (D_o - D_e) \star C_1. \quad (32)$$

The first term of eq. 31, when integrated over all  $x'$ ,

$$\int_0^\infty (D_o - D_e) d|x'| = \frac{\sqrt{3}(3x_0/z + x'_0)}{2\sqrt{\pi}\theta_s z^{3/2}} e^{-(3/\theta_s^2 z)(x_0/z + x'_0)^2} \quad (33)$$

corresponds to a Gaussian in the variable  $\alpha \equiv (x_0/z + x'_0)/\sqrt{z}$ , which, when integrated further over all  $z$ , again is equal to one half. It then follows that eq. 31 integrated over all  $x'$  and  $z$  likewise leads to the series of eq. 27.

In spite of the similarity, important differences remain with the edge-to-edge case. The  $z$ -distribution of eq. 33 is obviously more complicated than its counterpart of eq. 25. More troublesome is the observation that  $\int_0^\infty (D_o - D_e) d|x'|$  for the front-to-edge case becomes negative when  $x'_0 < 0$  and when  $z > -3x_0/x'_0$  ( $\equiv z_0$ ), whereas for edge entrance  $x'_0$ , and hence  $\int_0^\infty (C_o - C_e) d|x'|$ , is always positive. But since  $D_1$  represents a probability distribution it must be positive everywhere and therefore the integral of the remaining term of eq. 32,  $\int_0^\infty (D_o - D_e) \star C_1 d|x'|$ , must compensate for this.

For  $x'_0 > 0$ , both terms of eq. 32 are positive everywhere and MC selection of the  $z$  of a first passage proceeds much like for edge entrance. Each term of eq. 32, integrated over all  $x'$  and  $z$ , contributes one half to the total (unit) probability. A value of  $\alpha$  is chosen randomly from a half-Gaussian (eq. 33, for  $0 < \alpha < \infty$ ) and the corresponding  $z$  follows by solving the cubic equation  $z(\alpha) = 0$ , which for  $x'_0 > 0$  always has one real root ( $= z$ ) and two complex roots. With a probability of one half this  $z$  is also the  $z$  of the first passage. The conditional probability,  $D(x'|x = 0, x'_0, x_0, z)$ , for  $x'$  at a given  $z$  of the normalized  $(D_o - D_e)$  is

$$D(x'|x = 0, x_0, x'_0, z) = (4|x'|/\sqrt{z}\sqrt{\pi}\theta_s A) \cdot \left[ e^{-4(|x'|-A/2)^2/\theta_s^2 z} - e^{-4(|x'+A/2)^2/\theta_s^2 z} \right] \quad (34)$$

where  $A = x'_0 + 3x_0/z$ . For  $x'_0 > 0$ ,  $A$  is always positive and hence eq. 34 is always positive. (Eq. 34 is actually cast in a different form for efficient MC selection but this complication is omitted here.) The other term of eq. 32,  $(D_o - D_e) \star C_1$ , carries equal probability and is sampled by generating an edge-to-edge first passage from an intermediate  $z$ ,  $x'$  obtained from  $(D_o - D_e)$  in the above fashion.

For  $x'_0 < 0$  the correspondence between  $z$  and  $\alpha$  is shown in fig. 8. For  $|\alpha| < 2|x'_0|^{3/2}/3\sqrt{3}x_0$  there are three real roots of which one lies in the  $z > z_0$  region, where  $D_o - D_e < 0$ . For  $\alpha > 2|x'_0|^{3/2}/3\sqrt{3}x_0$  there is one real root and two complex roots. Eq. 33 still holds but has no longer the same straightforward probabilistic interpretation.  $D_o - D_e$  is negative for  $z > z_0$ ,

independent of  $\mathbf{x}'$ . Likewise, the integrand of  $(D_o - D_e) \star C_1$  is negative for values of the integration variable  $z_i > z_0$ . The *positive* part of  $D_o - D_e$  has a total probability

$$p_1 = \frac{1}{2} \left[ 1 + \operatorname{erf}(2|\mathbf{x}'_0|^{3/2}/3\sqrt{x_0}\theta_s) \right] \quad (35)$$

between 1/2 and unity. The MC proceeds by selecting, with probability  $p_1$ , a first passage from the positive part of  $D_o - D_e$  by choosing an  $\alpha$  from the truncated Gaussian of fig. 8 and solving  $z(\alpha)$ . The  $\mathbf{x}'$ -selection follows the  $\mathbf{x}'_0 > 0$  case. The remaining part of the probability,  $1 - p_1$ , is simulated by generating an edge-to-edge first passage  $z, \mathbf{x}'$  from an intermediate  $z_i, \mathbf{x}'_i$  ( $z_i < z_0$ ) obtained from (the positive part of)  $D_o - D_e$ . If  $z$  is less than  $z_0$ , then  $z, \mathbf{x}'$  can still be immediately identified as a (front-to-edge) first passage. For  $z > z_0$  a correction must be applied to account for the negative parts of both terms: eq. 32, rewritten with the convolution integral split into two parts,

$$D_1 = (D_o - D_e) + \int_0^{z_0} \int_0^\infty (D_o - D_e) \cdot C_1 dz_i d|\mathbf{x}'_i| + \int_{z_0}^z \int_0^\infty (D_o - D_e) \cdot C_1 dz_i d|\mathbf{x}'_i| \quad (36)$$

has a positive middle term while the first and third term are negative. Equivalently,

$$D_1 = \int_0^{z_0} \int_0^\infty (D_o - D_e) \cdot C_1 dz_i d|\mathbf{x}'_i| \cdot \left\{ 1 - \frac{(D_e - D_o) + \int_{z_0}^z \int_0^\infty (D_o - D_e) \cdot C_1 dz_i d|\mathbf{x}'_i|}{\int_0^{z_0} \int_0^\infty (D_o - D_e) \cdot C_1 dz_i d|\mathbf{x}'_i|} \right\} \quad (37)$$

whence the MC algorithm: sample  $z, \mathbf{x}'$  from  $(D_o - D_e) \star C_1$  ( $0 < z_i < z_0$ ) and take the factor in the braces into account using rejection.

An accurate evaluation of the integrals inside the braces at every occurrence in the MC would result in unacceptably slow execution. Instead they are evaluated by the MC method at only a few points. Making use of the expanded form of  $C_1$  guarantees faster convergence for comparable computational effort. From eq. 24 it follows that

$$(D_o - D_e) \star C_1 = [(D_o - D_e) + (D_o - D_e) \star (C_o - C_e) + \dots] \star (C_o - C_e). \quad (38)$$

The expression  $(C_o - C_e)$  at the end of eq. 38 is always directly evaluated while each of the terms of the series in the square brackets is generated by MC simulation.

To qualify as a rejection factor, the expression in braces must have a value between zero and unity. This is guaranteed from probability considerations but may not always hold for approximate values. However the MC algorithm requires the rejection factor to lie within this range and evaluation of the integrals continues until the criterion is met.

### 3.4 Back Escape

For a block of finite length, back escape, with entrance either via the edge or front of the block, is pictured schematically in fig. 9a. The problem is to find the coordinates and direction of the particle at the point of escape from the back of the block, in the presence of an edge. (Whether the particle will escape via the edge or back is decided in the MC by generating a first passage  $z, \mathbf{x}'$  and testing  $z$  versus the length of the block.) The back escape problem generalizes to include the problem of finding the coordinates and incident particle direction for a point process (see fig. 9b).

Only the case of front entrance-back escape is stated explicitly here but it readily specializes to side entrance-back escape. The MC algorithm adopted here is to choose  $\mathbf{x}, \mathbf{x}'$  from the Fermi distribution (eq. 15) and apply a correction factor to account for out-scattering. Call  $F_0(\mathbf{x}, \mathbf{x}')$  the distribution with the edge present, then

$$F_0(\mathbf{x}, \mathbf{x}') = F(\mathbf{x}, \mathbf{x}' | \mathbf{x}_0, \mathbf{x}'_0, z) - \int_0^z \int_0^\infty D_1(z_i, \mathbf{x}'_i | \mathbf{x}_0, \mathbf{x}'_0, 0) G(\mathbf{x}, \mathbf{x}' | \mathbf{x}'_i, z - z_i) dz_i d|\mathbf{x}'_i| \quad (39)$$

where a different symbol,  $G(\mathbf{x}, \mathbf{x}' | \mathbf{x}'_i, z - z_i)$ , signifies the special condition of edge entrance:  $\mathbf{x}_0 = 0$ . In the manner of eq. 37, this can be rewritten as the Fermi distribution times a rejection factor

$$F_0(\mathbf{x}, \mathbf{x}') = F(\mathbf{x}, \mathbf{x}' | \mathbf{x}_0, \mathbf{x}'_0, z) \cdot \left\{ 1 - \frac{\int_0^z \int_0^\infty D_1(z_i, \mathbf{x}'_i | \mathbf{x}_0, \mathbf{x}'_0, 0) G(\mathbf{x}, \mathbf{x}' | \mathbf{x}'_i, z - z_i) dz_i d|\mathbf{x}'_i|}{F(\mathbf{x}, \mathbf{x}' | \mathbf{x}_0, \mathbf{x}'_0, z)} \right\}. \quad (40)$$

The MC follows closely the algorithm discussed in connection with eq. 37. This appears, at least conceptually, the simplest way to account for the presence of the edge [25].

## 4 Results

The MC program ELSIM serves mainly to simulate realistic scenarios of beam loss and, with the help of other programs, its consequences. It appears nonetheless useful to present a few general results here, i.e., some results pertaining to a pencil beam incident on a block at various angles and displacements from the edge, without the complication of an extended incident phase space.

Figs. 10–13 show iso-absorption contour plots for 1 TeV/c protons in the space of  $x_0, x'_0$ , the incident particle's displacement and angle, for various materials. Each contour represents a certain fraction of particles absorbed ( $\Delta p \geq 1\%$ ) in a semi-infinitely long ( $0 < z < \infty$ ), semi-infinitely wide ( $0 < x < \infty, -\infty < y < \infty$ ) block. The remainder can then be interpreted as the fraction scattered out via the edge. This follows closely the presentation of Sievers [27], and there is at least qualitative agreement with ref. [27]. Better agreement is likely lacking because Sievers considers neither the edge regime nor wide angle processes in great detail. As is evident from the basic formulæ for (single or multiple) Coulomb scattering, angles and distances should scale with momenta as  $p^{-1}$ . This can be ascertained, e.g., by comparing fig. 12 with fig. 14 which represent iso-absorption curves for iron at 1 TeV/c and 20 TeV/c, respectively. The scaling is almost exact for small fractional absorption but deviations are clear for the iso-contours of 80% and above. This is presumably due to the non-Coulomb contributions which do not scale with the same precision. Under the rule adopted here, whereby particles with momentum loss exceeding 1 % of the incident momentum are excluded from the elastic regime, scaling is directly affected by target length and incident momentum, e.g., 100 GeV/c protons penetrating  $\sim 70$  cm of iron have lost on average  $\sim 1\%$  of their momentum due to collision losses only.

For many applications the intercept of the iso-absorption curves with the ordinate is of special interest since this corresponds to absorption probabilities of particles entering via the edge. This is shown in more detail in fig. 15 for 1 TeV/c protons. It can be seen that, for an infinitely long scraper, low- $Z$  materials are favored over high- $Z$  ones. For practical purposes these results hold for finite targets down to lengths of about one meter. For much shorter targets and for sufficiently large  $x'_0$  the heavier targets become more favorable. This is illustrated in fig. 16 which is similar to fig. 15 but pertains to a 20 cm long target. Both figs. 15 and 16 show, somewhat surprisingly, that absorption remains significant down to extremely small angles (where

some of the difficulties with the model, referred to above, are likely to come into play).

Variation of absorption probability with target length is pictured in fig. 17 which presents iso-absorption contours for the case of a 1 TeV/c proton beam incident on the edge on an iron target as a function of  $x'_0$  and  $z$ . Complementary to fig. 17, contours of equal back-escape from the same calculation are shown in fig. 18. By subtracting the combined results of figs. 17 and 18 from unity the probability of out-scattering via the edge is obtained. For the case of 1 TeV/c protons incident edgewise on an infinitely long iron target, a number of global averages pertaining to particles exiting the block are plotted in fig. 19 as function of the incident angle  $x'_0$ . Absorption and wide angle processes greatly reduce these averages in value and make their calculation tractable by the MC method. The first passage distribution for mCs alone (eq. 24) is marked by extremely long tails which make averaging difficult. Fig. 20 shows absorption probabilities of various materials for a 1 TeV/c proton pencil beam parallel to the edge ( $x'_0 = 0$ ) when the displacement from the edge is varied. Again it is observed that absorption remains significant even down to extremely small displacements from the edge. Again it is cautioned that at these extremes care must be taken in the interpretation of the results.

## 5 Concluding Remarks

In all cases examined here, when either or both  $x_0$  and  $x'_0$  are sufficiently large there is good agreement between calculations based on the above algorithms and stepwise simulation. When  $x_0$  and  $x'_0$  are both small, results diverge in an expected manner. (In some applications it may of course be advantageous to combine these two techniques.)

The MC algorithms derived here are all unweighted procedures. Weighting schemes become convenient and even necessary when attention is focussed on rare events. A generally applicable weighting technique has been mentioned in connection with deep penetration (sec. 2.6). In some instances it may be advantageous to replace rejection factors as occur, e.g., in eqs. 37 and 40, with weights. For many problems, however, efficient weighting schemes will tend to be more complex and are best constructed on an *ad hoc* basis.

As shown in sec. 3 the algorithms are easy to apply in a MC calculation. Even if closed form solutions were known to these problems, there

may be no computational gain since, on account of the complexity of the point processes, MC simulation offers the only practical means to study the complete problem and the closed form solutions would not necessarily lead to simpler algorithms. Other than for their statistical nature, characteristic of MC simulations, the algorithms represent the first passage distribution of mCs essentially to the same degree of approximation as the Fermi distribution does in a homogeneous target. Problems at large scattering angles, connected with the latter, are largely circumvented by the introduction of a sensibly small cut-off angle (see sec. 2.1).

Finally, expressions such as eqs. 24, 32, etc., are more general than their present application to mCs. They can serve to generate first passage distributions for any diffusion problem [26] for which the joint  $\mathbf{x}, \mathbf{x}'$  distribution is known along the boundary of interest, whatever its shape. Generalization to multiple boundaries and multiple material targets appears possible and rather straightforward for plane edges. As a practical matter the usefulness of the algorithms for other distributions and geometries will be determined by mathematical convenience.

## A Fermi Distribution

An alternative to the Eyges-Scott type derivation, based more directly on probability arguments, starts by observing that  $\mathbf{x}'$  executes a simple one-dimensional random walk consisting of a series of independent steps  $\Delta \mathbf{x}'_i = (\mathbf{x}'_i - \mathbf{x}'_{i-1})$ . For convenience set  $\mathbf{x}_0 = 0$  and  $\mathbf{x}'_0 = 0$ . From the Central Limit Theorem, after a sufficiently large distance,  $Z$ , the variable  $\mathbf{x}' (= \sum \Delta \mathbf{x}'_i$ , for  $\mathbf{x}'_0 = 0$ ) has a Gaussian distribution with  $\overline{\mathbf{x}'} = 0$ ,  $\sigma_{\mathbf{x}'} = \theta_s Z^{1/2} / \sqrt{2}$  where  $\theta_s$  is the rms (spatial) angle of scattering per unit length (see sec. 2.1) and where  $Z^{1/2}$  appears because to obtain the rms  $\mathbf{x}'$  the  $\Delta \mathbf{x}'_i$  add in quadrature

$$P(\mathbf{x}') = \frac{1}{\sqrt{\pi} \theta_s Z^{1/2}} e^{-\mathbf{x}'^2 / \theta_s^2 Z}. \quad (41)$$

The displacement,  $\mathbf{x}$ , is likewise a linear combination of the  $\Delta \mathbf{x}'_i$

$$\mathbf{x} = Z \mathbf{x}'_0 + (Z - z_1) \Delta \mathbf{x}'_1 + \dots + (Z - z_n) \Delta \mathbf{x}'_n = \sum_{i=1}^n (Z - z_i) \Delta \mathbf{x}'_i \quad (42)$$

where the second equality follows from the choice  $\mathbf{x}'_0 = 0$ . The index  $i$  enumerates the scatterings or may also refer to some fixed large number of equidistant ( $\Delta z$ ) points between 0 and  $Z$ . Using the latter interpretation it

follows that the  $\Delta x'_i$  are normally distributed with  $\overline{\Delta x'_i} = 0$  and  $\sigma_{\Delta x'_i}^2 = \theta_s^2 \Delta z / 2$  and that likewise  $x$  is normally distributed with  $\bar{x} = 0$  and

$$\sigma_x^2 = \sum (Z - z_i)^2 \sigma_{\Delta x'_i}^2 = \sum (Z - z_i)^2 \theta_s^2 \Delta z / 2 \quad (43)$$

since the  $\Delta x'_i$  are independent. In the limit of  $\Delta z \rightarrow 0$

$$\sigma_x^2 = \frac{\theta_s^2}{2} \int_0^Z (Z - z)^2 dz = \frac{\theta_s^2}{2} \cdot \frac{Z^3}{3} \quad (44)$$

as can be verified in sec. 3.1.

Since both  $x'$  and  $x$  are linear combinations of independently normally distributed variables (the  $\Delta x'_i$ ), their joint distribution is guaranteed to be (bivariate) normal with  $\sigma_x, \sigma_{x'}$  as for the marginal distributions (eqs. 41 and 44) [28]. There remains only to determine the coefficient of correlation,  $\rho$ , between  $x'$  and  $x$ , which, for  $\bar{x}' = 0, \bar{x} = 0$ , can be written as  $\rho = \overline{x'x} / \sigma_{x'} \sigma_x$ . From eq. 42,

$$\rho = \frac{(\sum (Z - z_i) \Delta x'_i) \cdot (\sum \Delta x'_i)}{\sigma_{x'} \sigma_x} = \frac{\sum (Z - z_i) (\Delta x'_i)^2}{\sigma_{x'} \sigma_x} \quad (45)$$

which becomes in the limit  $\Delta z \rightarrow 0$

$$\rho = \frac{\int_0^Z (\theta_s^2 / 2) (Z - z) dz}{\theta_s^2 Z^2 / 2\sqrt{3}} = \sqrt{3}/2. \quad (46)$$

The Fermi distribution is obtained by substituting  $\sigma_x, \sigma_{x'}$  and  $\rho$  in the general form of the bivariate normal distribution of  $x$  and  $x'$

$$F(x, x'|0, 0, Z) = (2\sqrt{3}/\pi\theta_s^2 Z^2) e^{-(4/\theta_s^2 Z)(x'^2 - 3x'x/Z + 3x^2/Z^2)} \quad (47)$$

which corresponds to eq. 15 with  $x_0 = x'_0 = 0$ . Generalization to eq. 15 follows from geometrical arguments.

## Acknowledgments

My thanks to D. Edwards for helpful criticism of the manuscript. Likewise to M. Harrison who also provided valuable scrutiny by using the program in the real world of the Tevatron.

## References

- [1] A. Van Ginneken, Fermilab FN-272 (1975).
- [2] A. Van Ginneken et al., to appear in *High Energy Hadron Colliders*, eds. A. Chao et al. (AIP New York, 1987).
- [3] See e.g. J. D. Jackson, *Classical Electrodynamics*, 2nd ed. (Wiley, New York, 1975) p. 674ff.
- [4] R. J. Glauber, *Lectures in Theoretical Physics*, eds., W. E. Brittin et al., Vol. 1 (Interscience, New York, 1959) p. 315ff; R. J. Glauber, *High Energy Physics and Nuclear Structure*, ed. G. Alexander, (North-Holland, Amsterdam, 1967) p. 311 ff; R. J. Glauber, *High Energy Physics and Nuclear Structure*, ed. S. Devons, (Plenum Press, New York, 1970) p. 207ff.
- [5] R. J. Glauber and G. Matthiae, Nucl. Phys. B21 (1970) 133.
- [6] G. Molière, Z. Naturforsch. 3a (1948) 78; H. A. Bethe, Phys. Rev. 89 (1953) 1256.
- [7] G. Shen et al., Phys. Rev. D20 (1979) 1584.
- [8] M. Holder et al., Phys. Lett. 36B (1971) 1; G. Barbiellini et al., Phys. Lett. 39B (1972) 663; U. Amaldi et al., Phys. Lett. 43B (1973) 231; D. S. Ayres et al., Phys. Rev. D15 (1977) 3105; L. Baksay et al., Nucl. Phys. B141 (1978) 1; L. A. Fajardo et al., Phys. Rev. D24 (1981) 46; R. Battiston et al., Phys. Lett. 115B (1982) 333.
- [9] G. Bellettini et al., Nucl. Phys. 79 (1966) 609.
- [10] A. Schiz, *Hadron-Nucleus Scattering at 70, 125, and 175 GeV/c and High Statistics Study of Hadron Proton Elastic Scattering at 200 GeV/c*, Thesis, Yale University (1979); A. Schiz et al., Phys. Rev. D21 (1980) 3010.
- [11] R. Herman and R. Hofstadter, *High Energy Electron Scattering Tables*, (Stanford University Press, Stanford, CA, 1960).
- [12] K. Goulianos, Phys. Repts 101 (1983) 169.
- [13] M. G. Albrow et al., Nucl. Phys. B108 (1976) 1.

- [14] M. Bozzo et al., Phys. Lett. 155B (1985) 197.
- [15] see e.g. R. D. Field and G. C. Fox, Nucl. Phys. B80 (1974) 367.
- [16] H. A. Bethe, Ann. Phys. 5 (1930) 325; F. Bloch, Z. Physik 81 (1933) 363; R. M. Sternheimer, Phys. Rev. 103 (1956) 511; R. M. Sternheimer et al., Atomic Data and Nuclear Data Tables 30 (1984) 261.
- [17] A. Van Ginneken, Nucl. Inst. Meth. A251 (1986) 21.
- [18] J. Bertrand, Comp. Rend. Acad. Sci. Paris 105 (1887) 369; D. André, Comp. Rend. Acad. Sci. Paris 105 (1887) 436.
- [19] see e.g., S. Chandrasekhar, Rev. Mod. Phys. 15 (1943) 1.
- [20] B. Rossi and K. Greisen, Phys. Rev. 70 (1946) 821. The term *distribution* with regards to eq. 15 is conventional in the physics literature but is called a *density* in probability texts.
- [21] L. Eyges, Phys. Rev. 74 (1948) 1534.
- [22] W. T. Scott, Phys. Rev. 76 (1949) 212.
- [23] When  $y$  is not infinite in both directions the problem remains tractable by treating the  $x$ -edge and  $y$ -edge independently and performing the MC 'in parallel'.
- [24] The distribution  $C_1$  can be represented in a variety of other ways, e.g.,

$$C_1 = C_o - C_e \star C_o + C_e \star C_e \star C_o - C_e^{\star 3} \star C_o + \dots$$

or

$$C_1 = (C_o + C_e) - (C_o + C_e)^{\star 2} + (C_o + C_e)^{\star 3} - \dots$$

The advantage of eq. 24 for the present application lies in the properties exhibited by eqs. 25–27 which lead to a convenient algorithm to simulate first passages in a MC calculation.

- [25] As another possibility, consider the case of side entrance with  $G_0(x, x')$  corresponding to  $F_0(x, x')$  (see eq. 39 with  $x_0 = 0$  and with  $C_1$  replacing  $D_1$ ). It can be verified that

$$G_+(x, x') = G_0(x, x'|x'_0, z) + \int_0^z \int_0^\infty C_e(x'_i, z_i|0, x'_0, 0) G_0(x, x'|x'_i, z - z_i) dz_i d|x'_i|$$

where  $G_+(x, x') = F(x, x'|0, x'_0, z)$  with  $x > 0$ . If one defines  $G_-(x, x') = F(-x, -x'|0, x_0, z)$  for  $x > 0$  then one can write

$$G_- = C_o \star G_0.$$

In combination with the expression for  $G_+$

$$G_0 = (G_+ - G_-) + (C_o - C_e) \star G_0$$

and by iteration

$$G_0 = (G_+ - G_-) + C_1 \star (G_+ - G_-).$$

For  $x_0 \neq 0$ , the analogous expression is

$$F_0 = (F_+ - F_-) + D_1 \star (G_+ - G_-).$$

The last two relations exhibit most clearly the connection to Kelvin's method. An explicit algorithm based on this approach has not been worked out mainly because of the presence of negative terms in expressions for probabilities which proved to be rather cumbersome in the front-to-edge problem.

- [26] It is interesting to connect eq. 32 with the well known first passage distribution for Brownian motion. A particle reaching an imaginary boundary in one dimensional Brownian motion is expected to cross this boundary a large number of times in the immediate vicinity before diffusing away from it. This means the  $C_1$  distribution can be approximated by a  $\delta$ -function. For a set of particles initially at  $x_0$  and for a boundary at  $x = 0$ , one obtains upon substituting  $\delta(z)$  for  $C_1$  in eq. 32, the first passage distribution

$$D_1 = 2(D_o - D_e).$$

$(D_o - D_e)$  is interpreted here as the net particle flux across the  $x = 0$  boundary, due to spreading of the Gaussian. This results in

$$D_1 = \frac{2x_0}{\sqrt{\pi}\theta_s z^{3/2}} e^{-x_0^2/\theta_s^2 z}$$

which is (cfr eq. 25) the stable distribution of index 1/2 and is usually derived from combinatorial arguments [19]. Inspection of this result confirms that for  $x_0 = 0$ ,  $D_1$  becomes indeed a  $\delta$ -function.

[27] P. Sievers, CERN Note Lab.II/BT/74-5 (1974).

[28] for a proof of this see M. C. Wang and G. E. Uhlenbeck, Rev. Mod. Phys. 17 (1945) 323.

## Figure Captions

- Fig. 1 Fit of  $K$  (or  $\theta_{min}$ ) to data of ref. 7. Error bars reflect experimental uncertainty.
- Fig. 2 Fits of Glauber theory to  $d\sigma/dt$  data of ref. 10 for elastic and quasi-elastic scattering (solid lines) of 70 GeV/c protons on various nuclear targets. Dashed lines include diffractive low mass target excitation.
- Fig. 3 Fits of Glauber theory to  $d\sigma/dt$  data of ref. 10 for elastic and quasi-elastic scattering (solid lines) of 175 GeV/c protons on various nuclear targets. Dashed lines include diffractive low mass target excitation.
- Fig. 4 Total cross section for p-p single diffraction dissociation and for compound single diffraction dissociation of protons on nuclear targets.
- Fig. 5 Trajectory crossing (a) virtual boundary in homogeneous medium, (b) edge of block into void. For (b) particle flux at point  $P$  is reduced. Trajectories (here and below) are drawn *schematically* only.
- Fig. 6 Particle entering semi-homogeneous target via flat edge. The distribution of particles emerging from the block as a function of  $z$  and  $x'$  is to be determined.
- Fig. 7 Schematic trajectory of particle repeatedly crossing a plane in a homogeneous target. The index  $j$  is attached to the  $j^{th}$  crossing.
- Fig. 8 Gaussian distribution of the variable  $\alpha$  and relation of  $\alpha$  to  $z$ . Trigonometric solutions of  $z(\alpha)$  with  $k = 1$  or  $2$  correspond to  $D_o - D_e > 0$  and are equi-probable;  $k = 0$  solution, corresponding to  $D_o - D_e < 0$ , appears in rejection factor (eq. 37).
- Fig. 9 (a) Back escape for front or edge entrance. (b) Equivalence of determining  $x, x'$  at point of interaction to determining  $x, x'$  at escape.
- Fig. 10 Iso-absorption contours for infinitely long, semi-infinitely wide ( $0 < x < \infty, -\infty < y < \infty$ ) *beryllium* target for a 1 TeV/c pencil

beam of protons as a function of displacement  $x_0$  and angle  $x'_0$  of the beam ( $y_0 = y'_0 = 0$ ).

Fig. 11 Iso-absorption contours for infinitely long, semi-infinitely wide *aluminum* target for a  $1 \text{ TeV}/c$  pencil beam of protons as a function of displacement  $x_0$  and angle  $x'_0$  of the beam.

Fig. 12 Iso-absorption contours for infinitely long, semi-infinitely wide *iron* target for a  $1 \text{ TeV}/c$  pencil beam of protons as a function of displacement  $x_0$  and angle  $x'_0$  of the beam.

Fig. 13 Iso-absorption contours for infinitely long, semi-infinitely wide *tungsten* target for a  $1 \text{ TeV}/c$  pencil beam of protons as a function of displacement  $x_0$  and angle  $x'_0$  of the beam.

Fig. 14 Iso-absorption contours for infinitely long, semi-infinitely wide *iron* target for a  $20 \text{ TeV}/c$  pencil beam of protons as a function of displacement  $x_0$  and angle  $x'_0$  of the beam.

Fig. 15 Fraction of protons absorbed in infinitely long, semi-infinitely wide targets of various materials, as a function of angle ( $x'_0$ ) of the  $1 \text{ TeV}/c$  proton beam incident on edge of target.

Fig. 16 Fraction of protons absorbed in a  $20 \text{ cm}$  long, semi-infinitely wide targets of various materials, as a function of angle ( $x'_0$ ) of the  $1 \text{ TeV}$  proton beam incident on edge of target.

Fig. 17 Iso-absorption contours for semi-infinitely wide *iron* target for a  $1 \text{ TeV}/c$  pencil beam of protons incident on edge of target as a function of angle ( $x'_0$ ) and target length ( $z$ ).

Fig. 18 Fraction of protons absorbed in infinitely long, semi-infinitely wide targets of various materials, as a function of displacement ( $x_0$ ) of the  $1 \text{ TeV}/c$  proton beam parallel to edge of target.

Fig. 19 Contours of equal back-escape probability for semi-infinitely wide *iron* target for  $1 \text{ TeV}/c$  pencil beam of protons incident on edge as a function of angle and target length ( $z$ ).

Fig. 20 Average  $x'$ ,  $\sigma_{x'}$ , average  $z$ ,  $\sigma_z$  and  $\sigma_y$  for infinitely long, semi-infinitely wide *iron* target for a  $1 \text{ TeV}/c$  pencil beam of protons incident on edge as a function of angle ( $x'_0$ ).

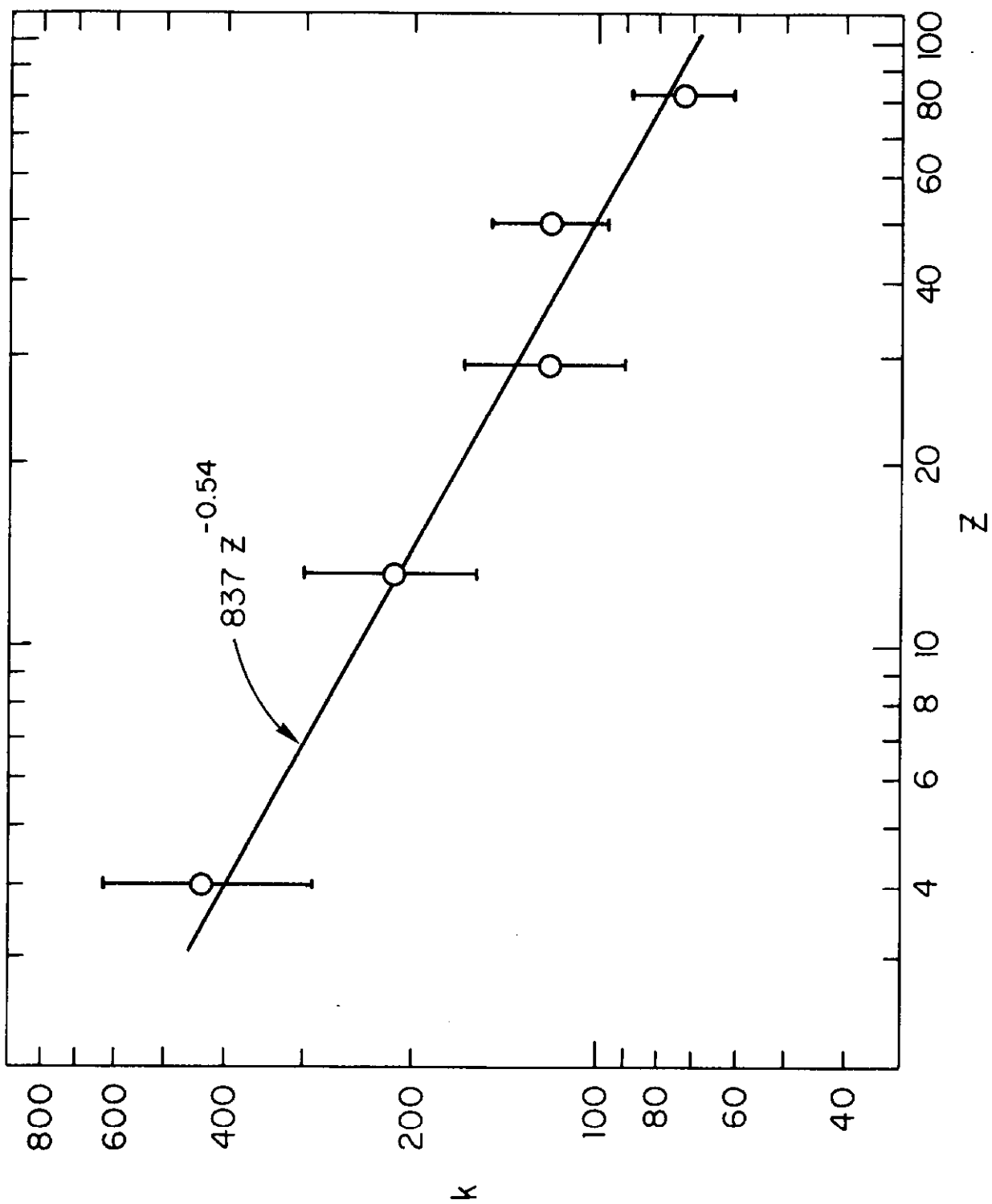


Fig. 1

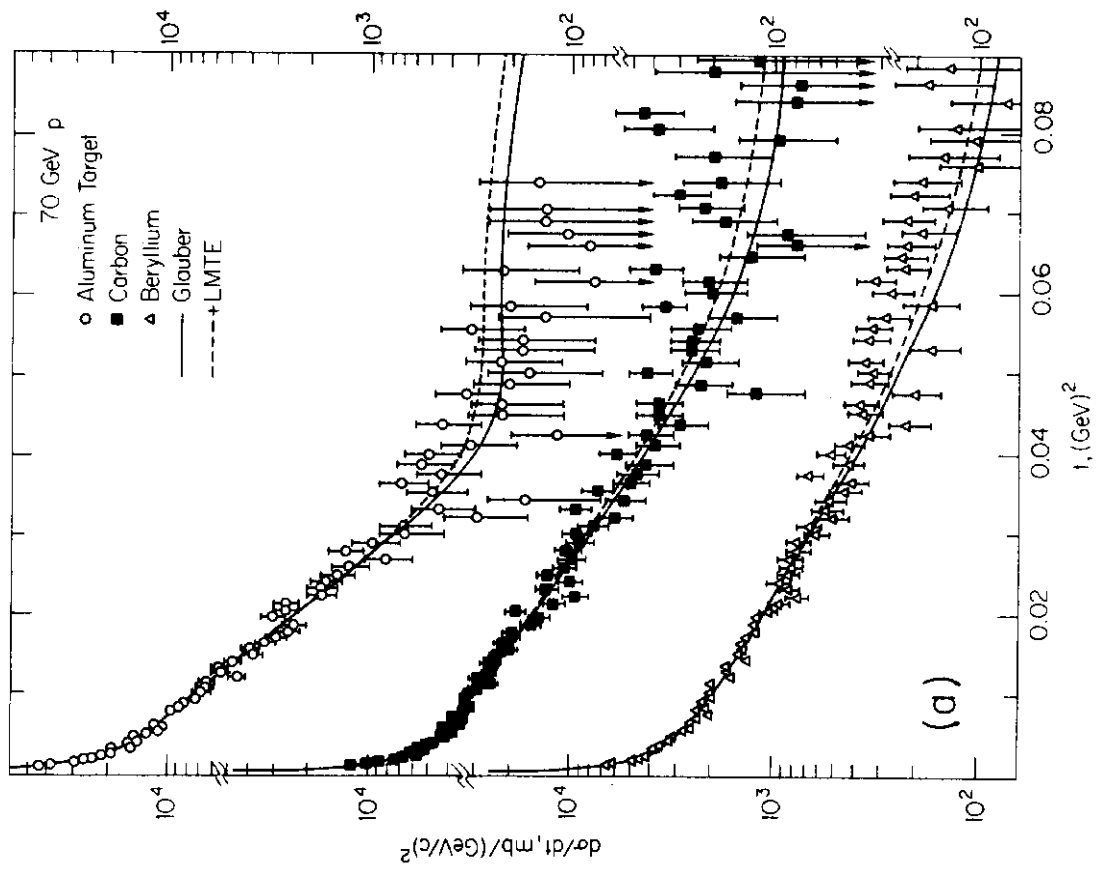
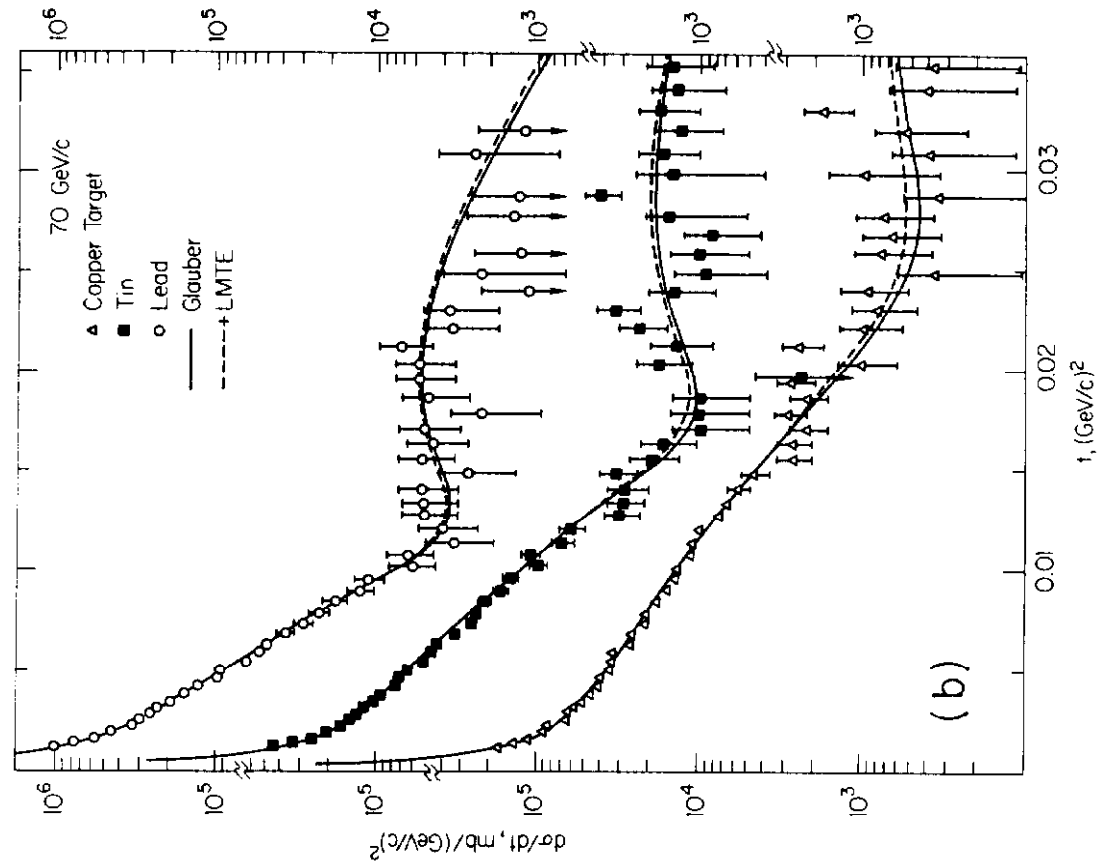


Fig. 2

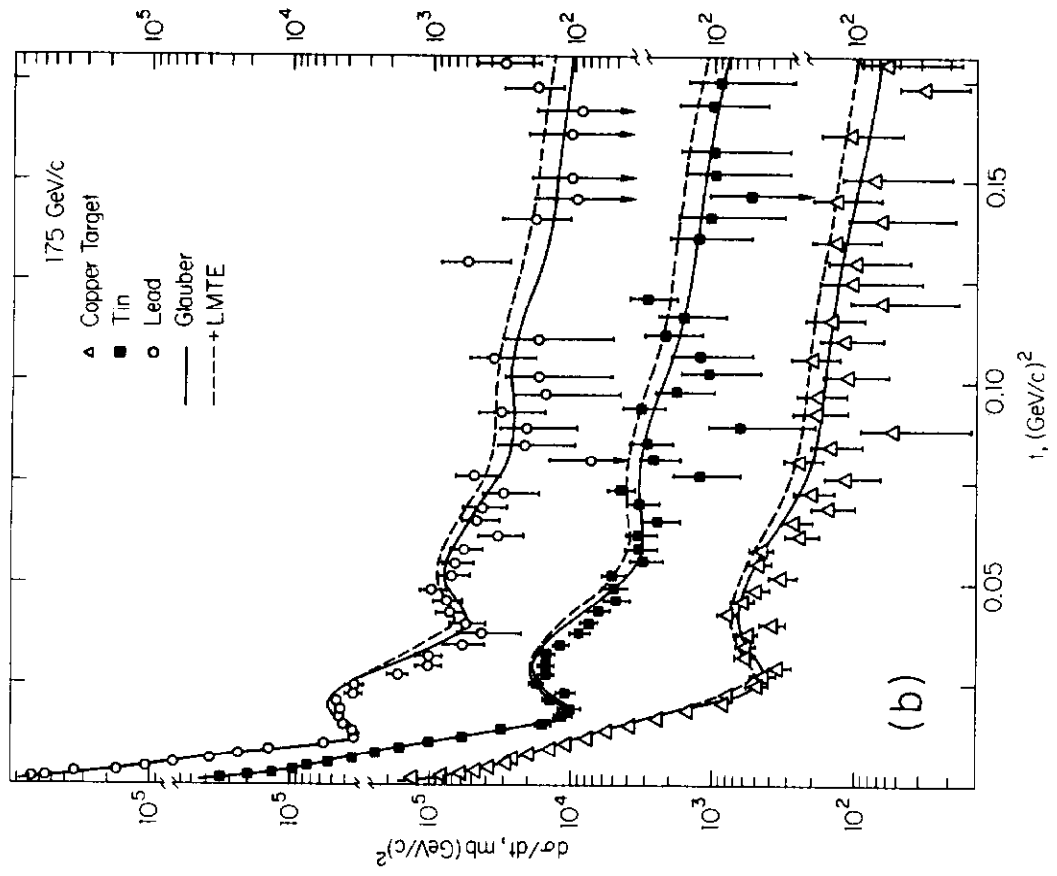
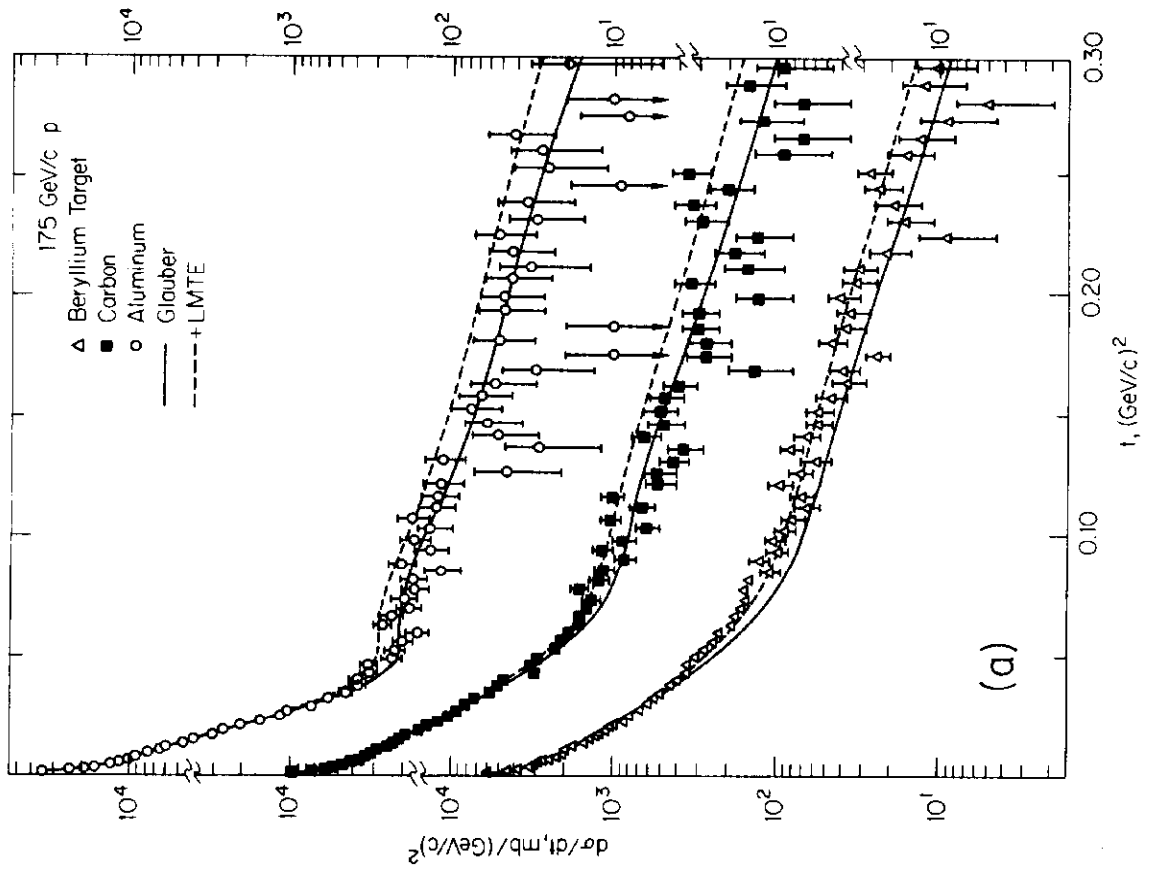


Fig. 3

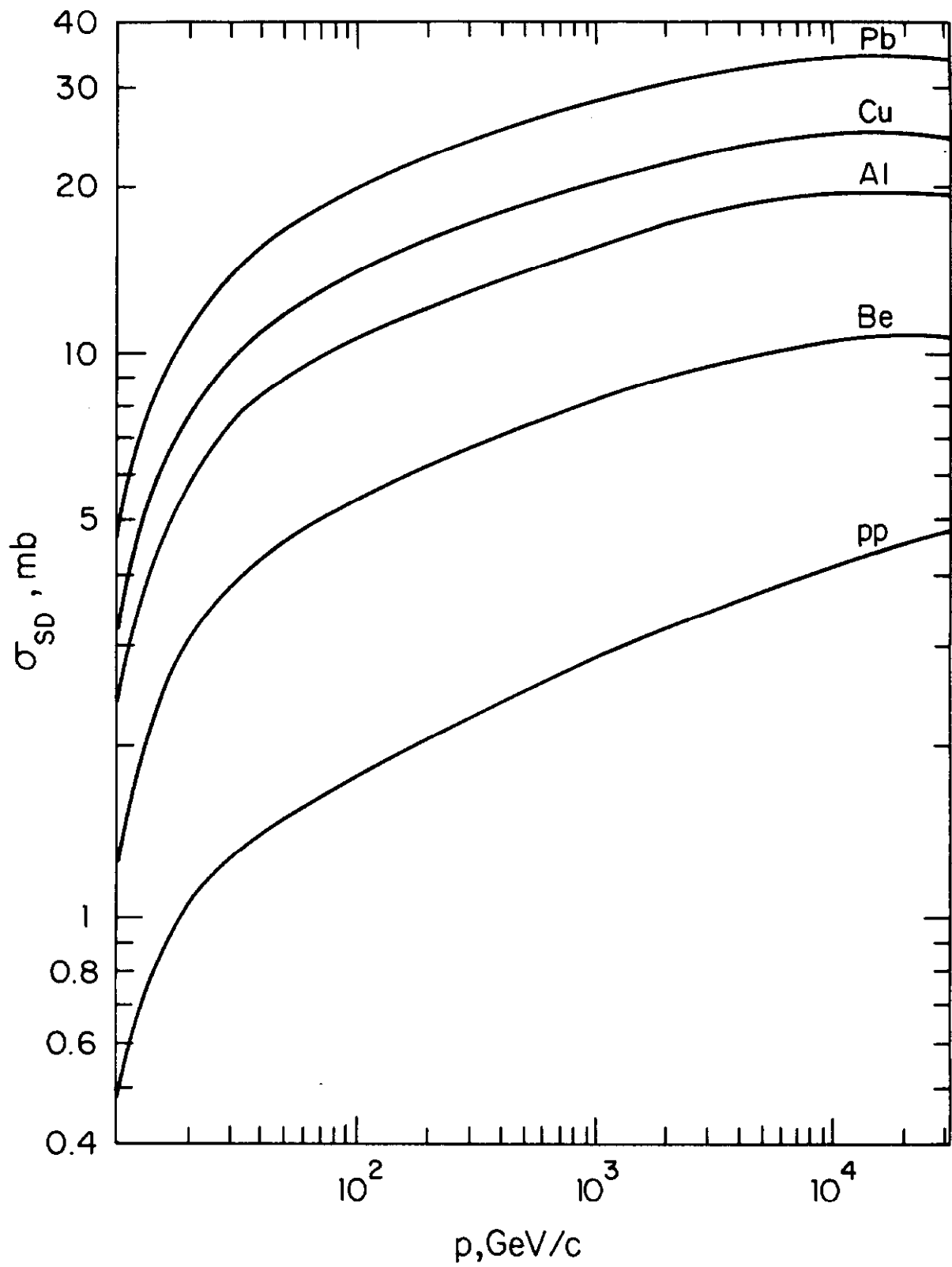


Fig. 4

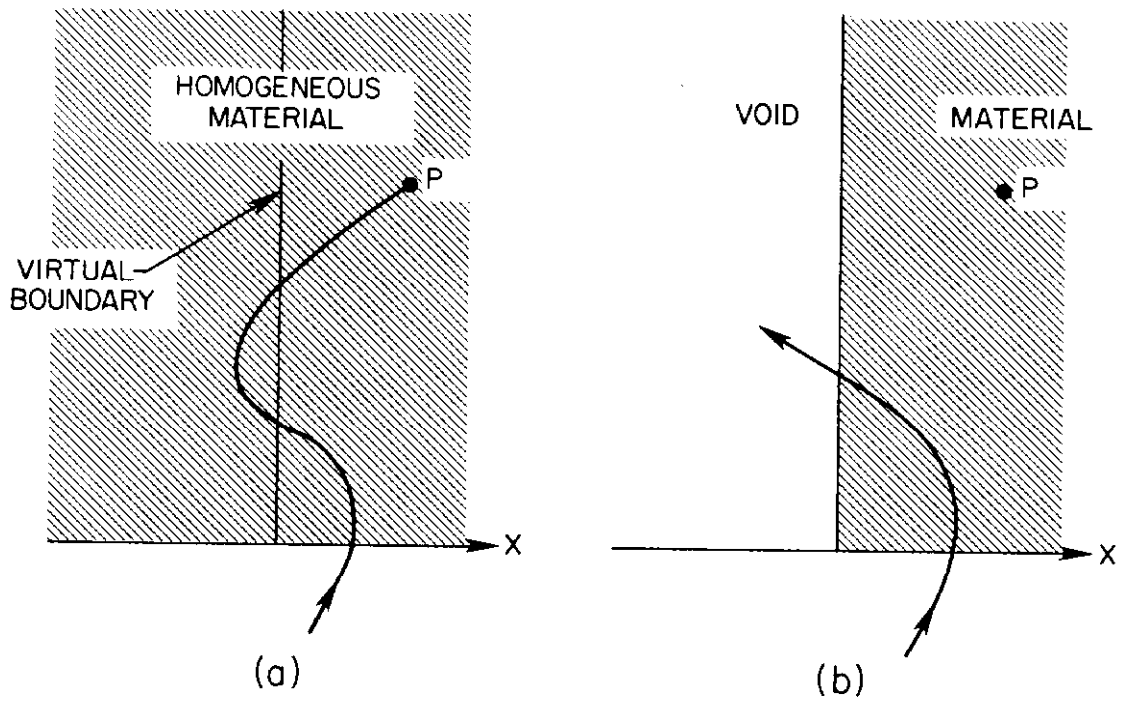


Fig. 5

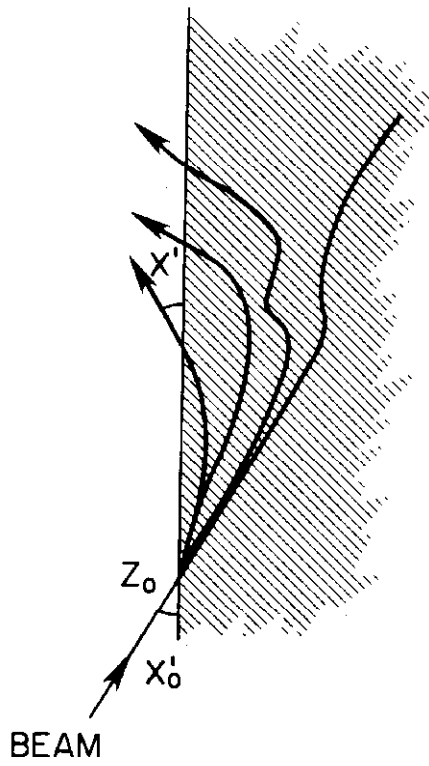


Fig. 6

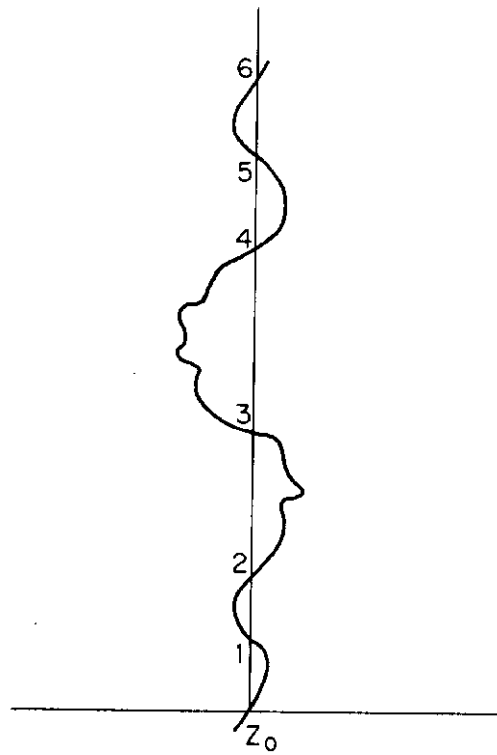


Fig. 7

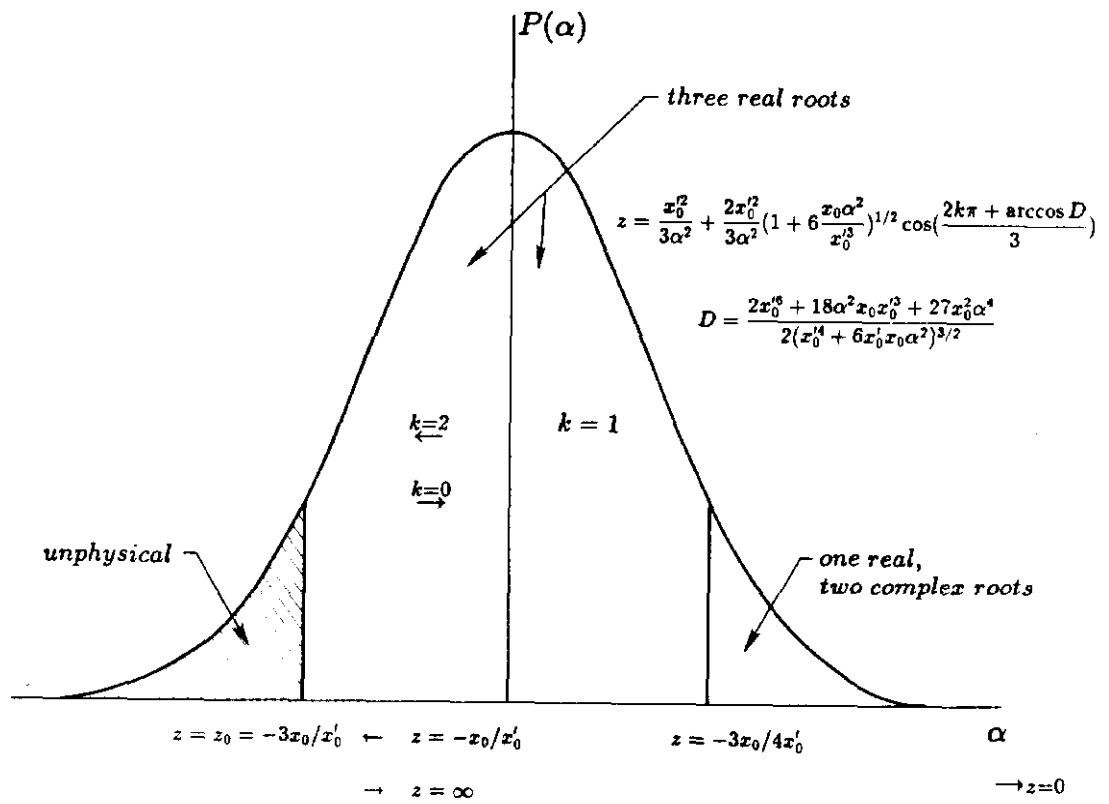


Fig. 8

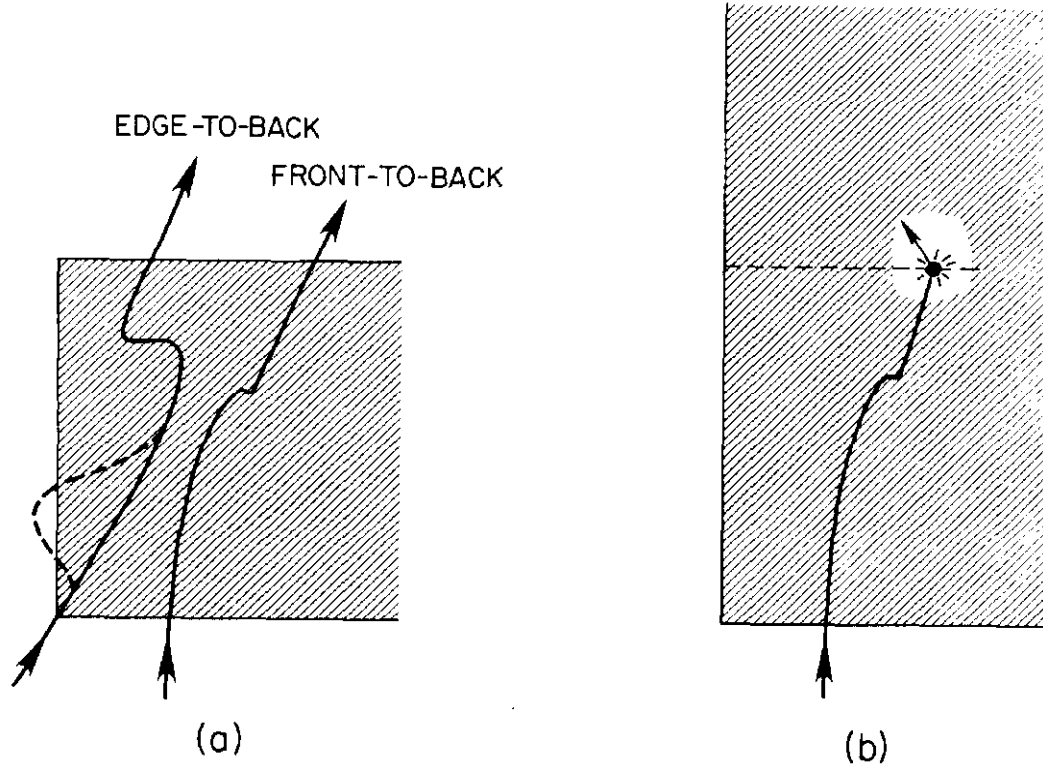


Fig. 9

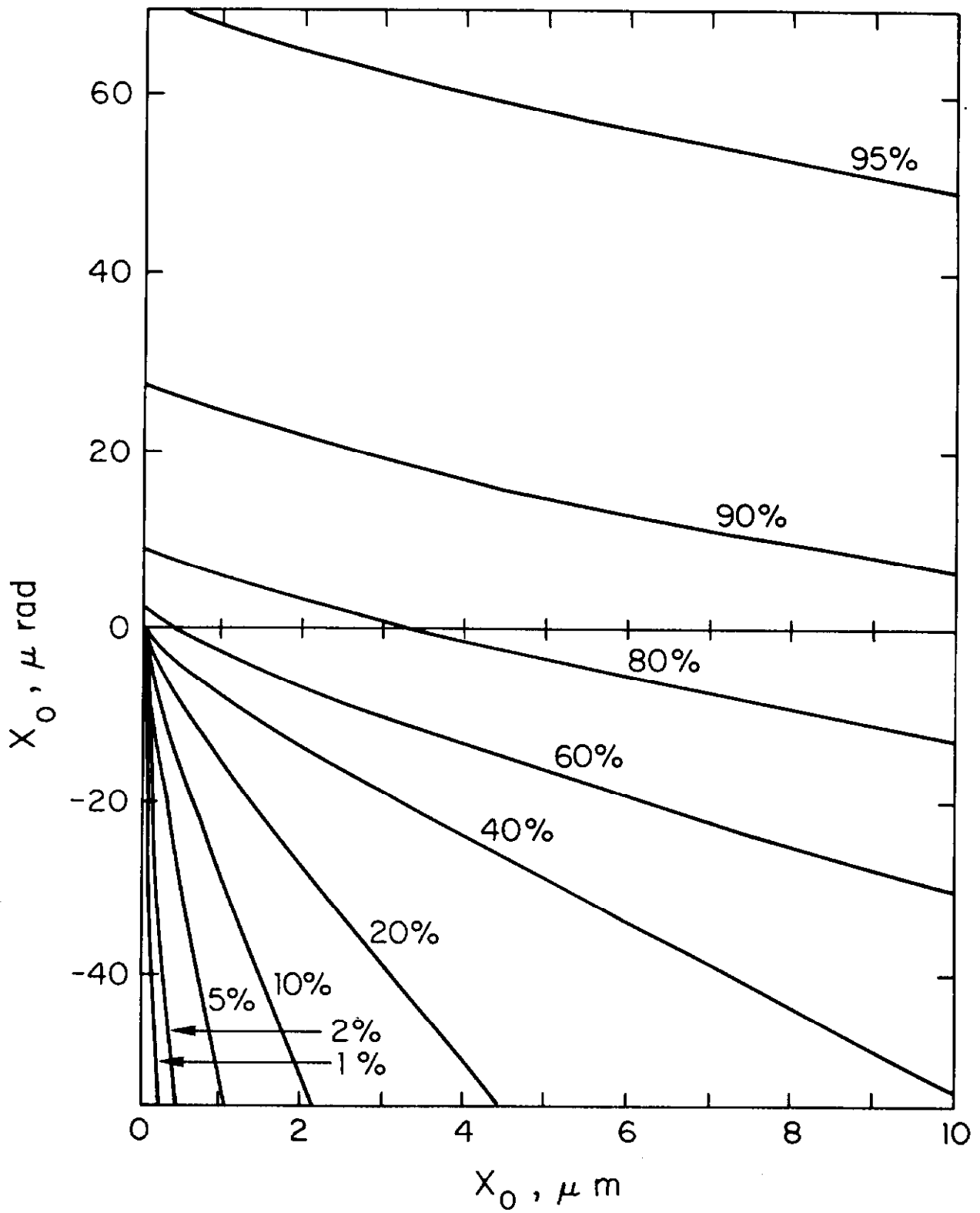


Fig. 10

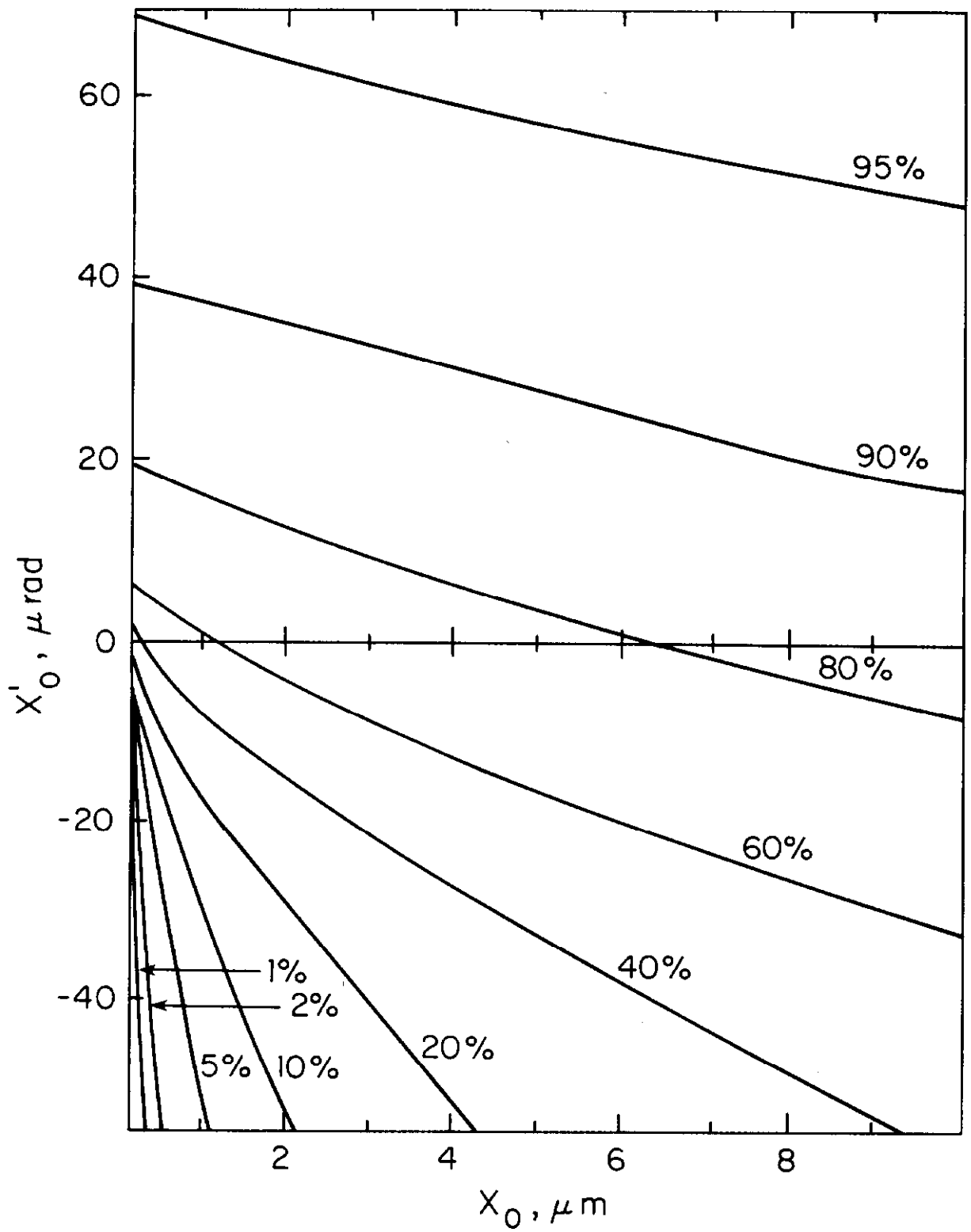


Fig. 11

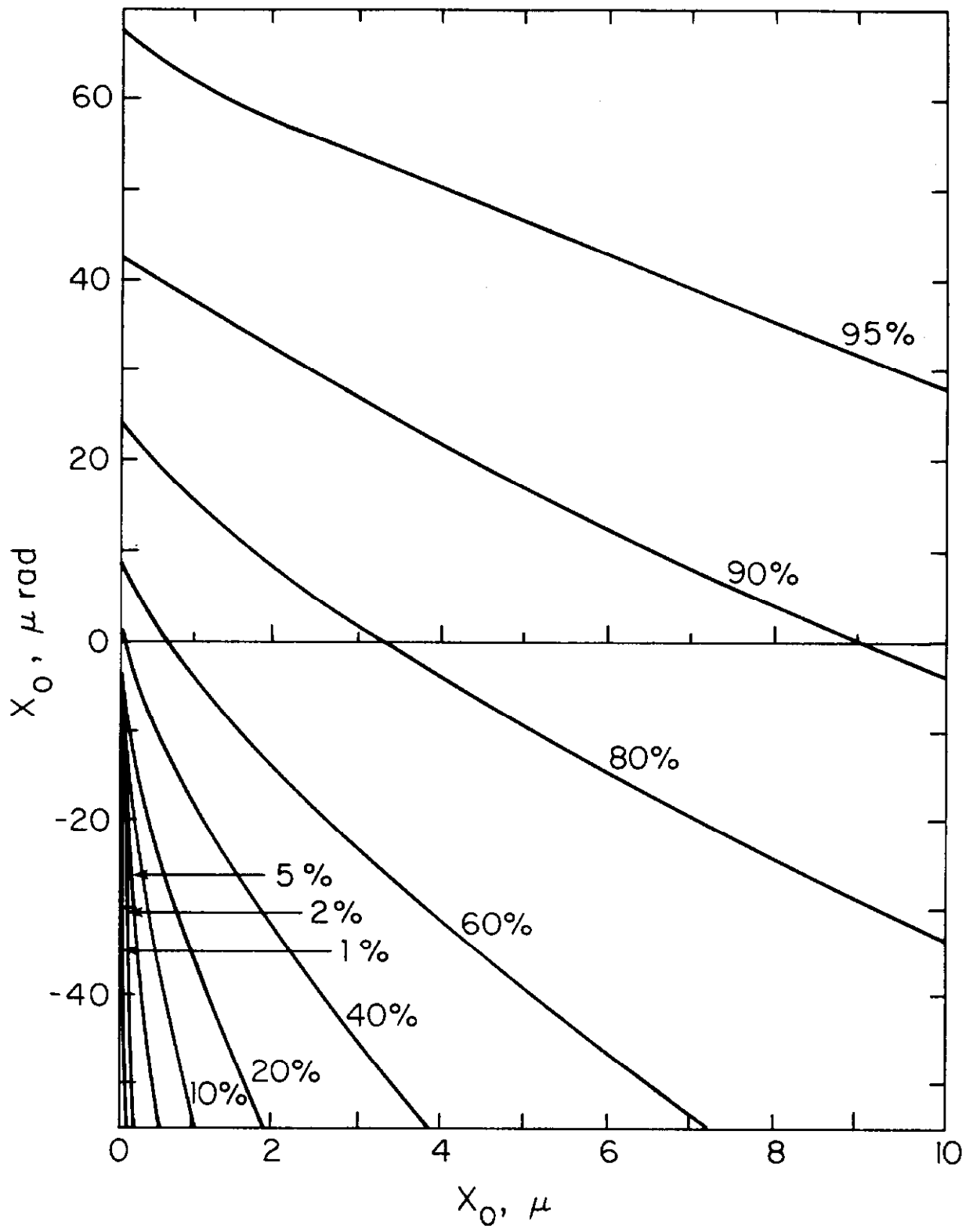


Fig. 12

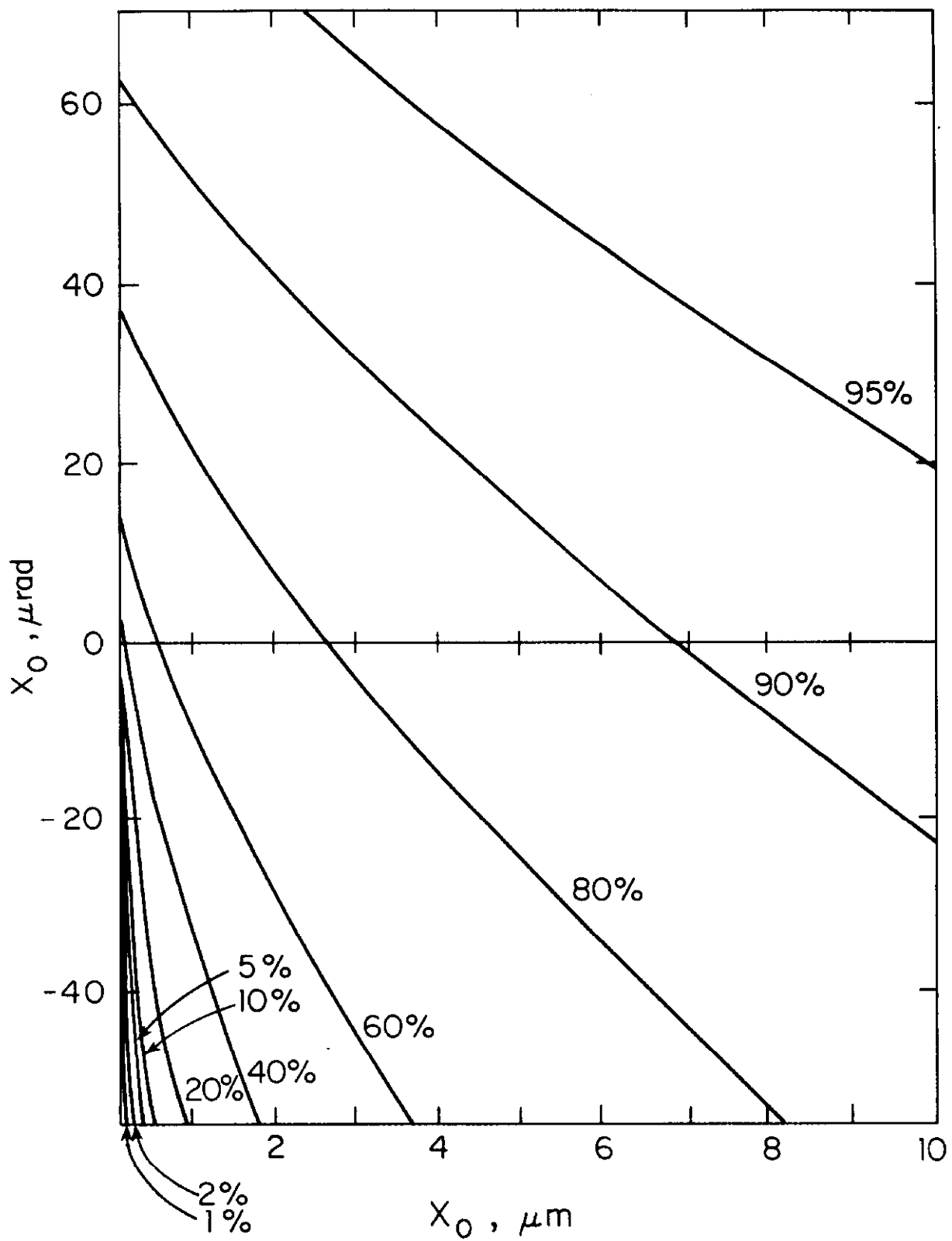


Fig. 13

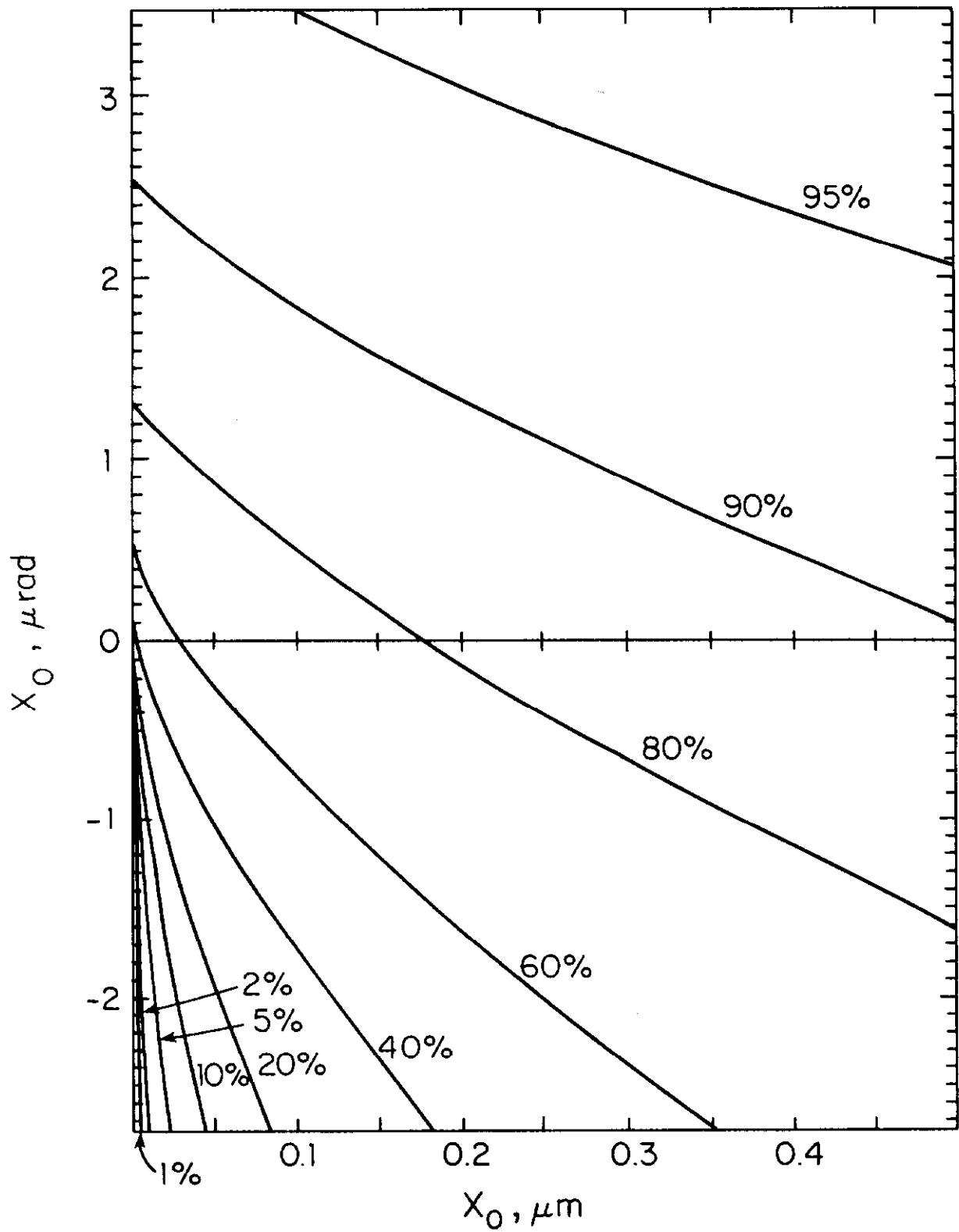


Fig. 14

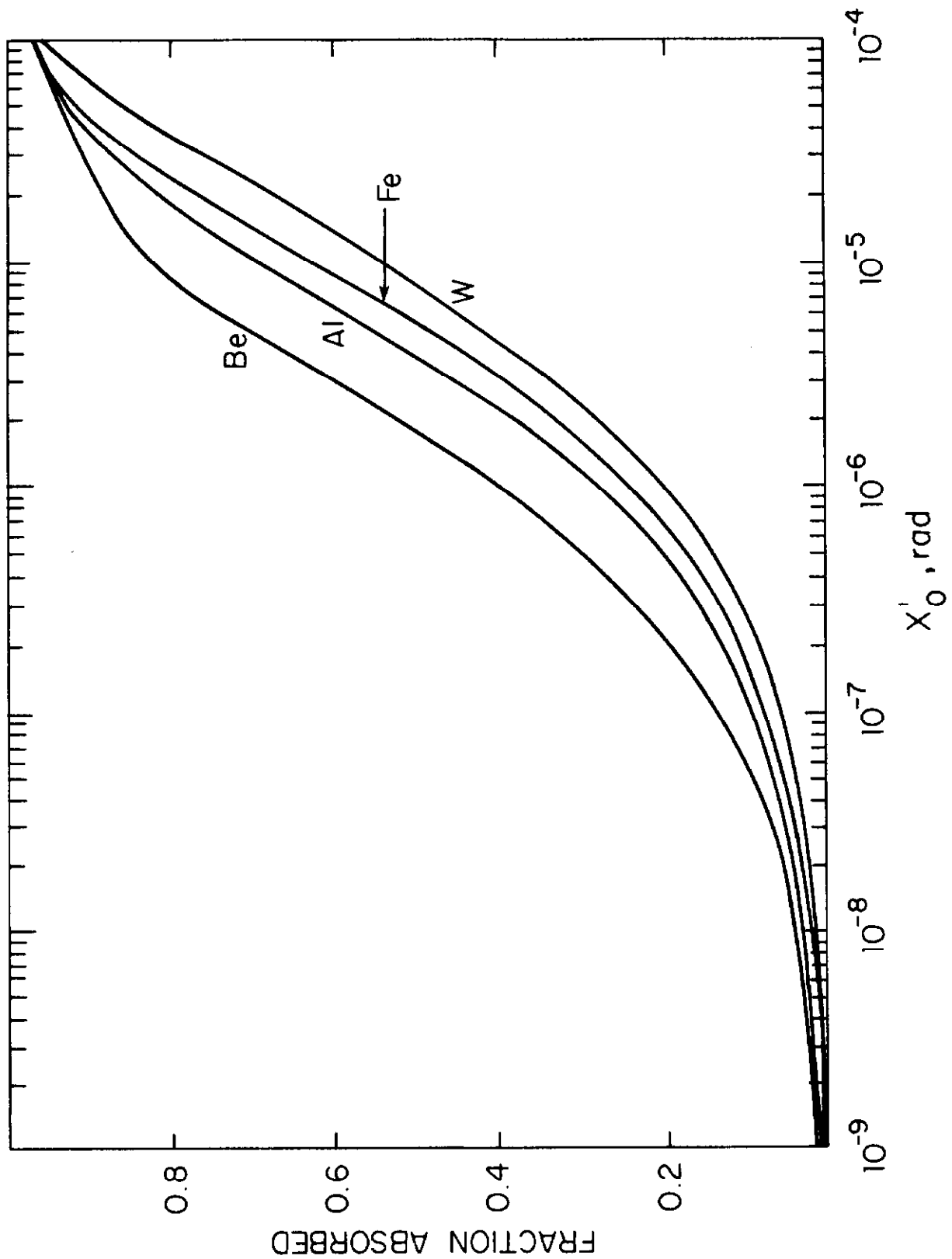


Fig. 15

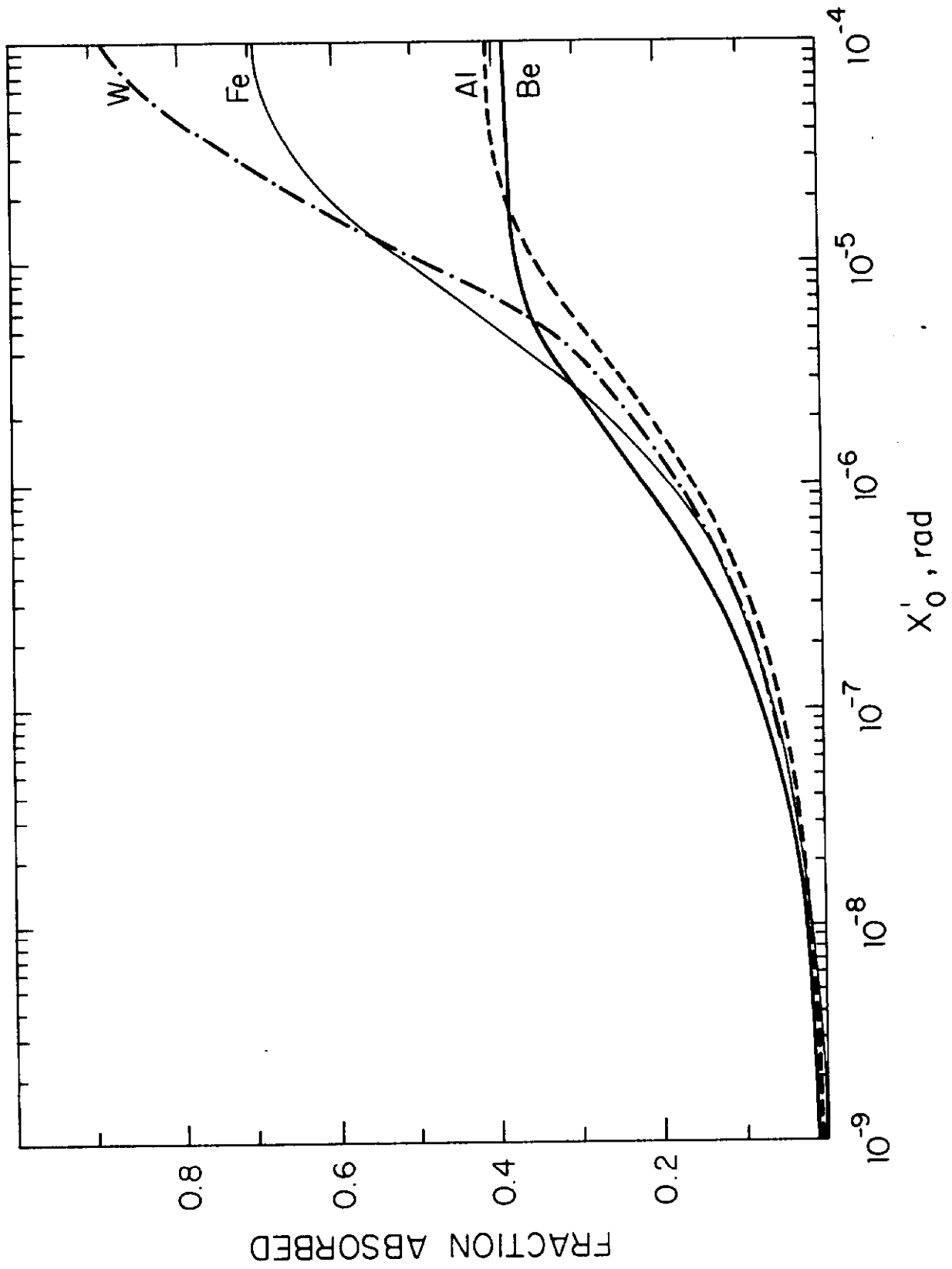


Fig. 16

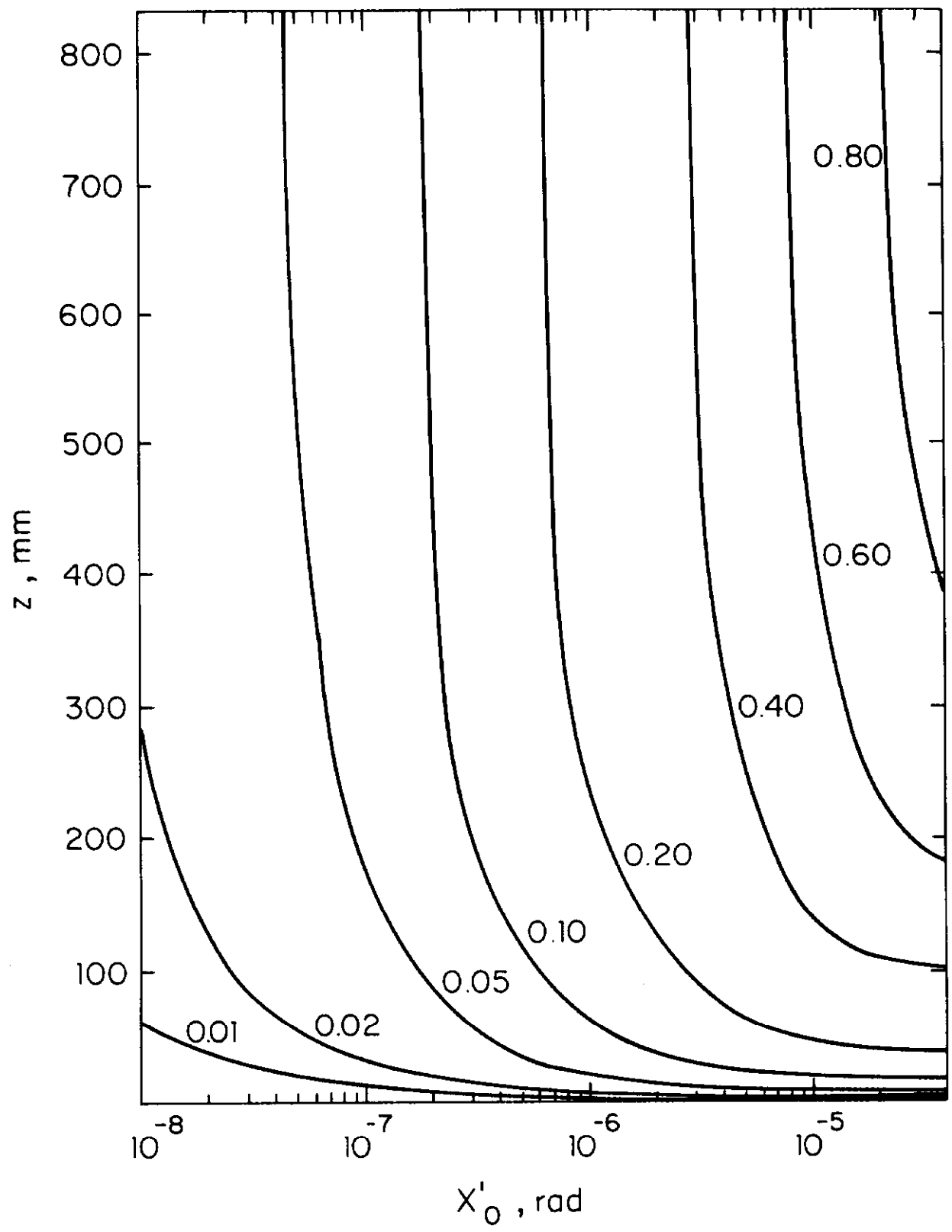


Fig. 17

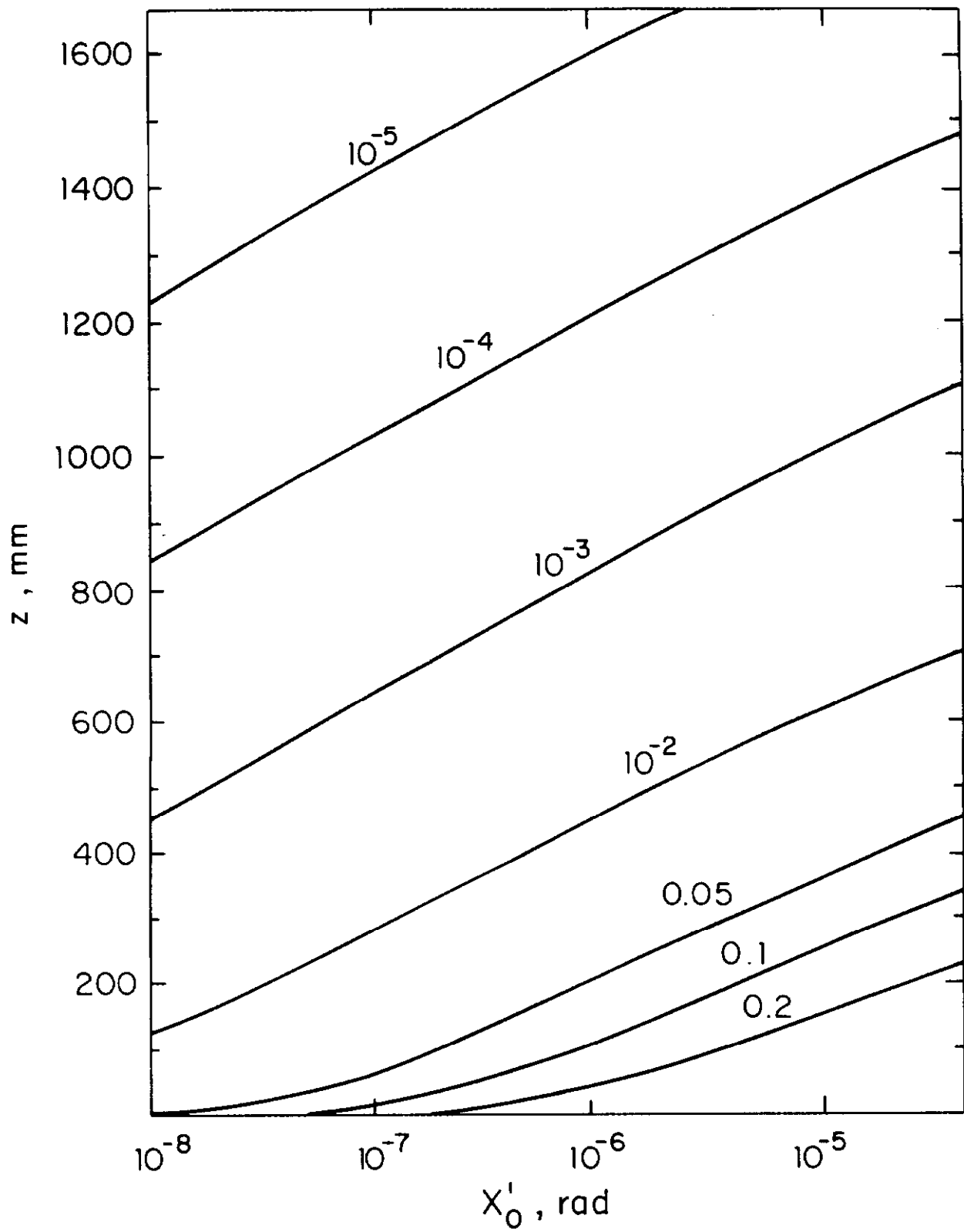


Fig. 18

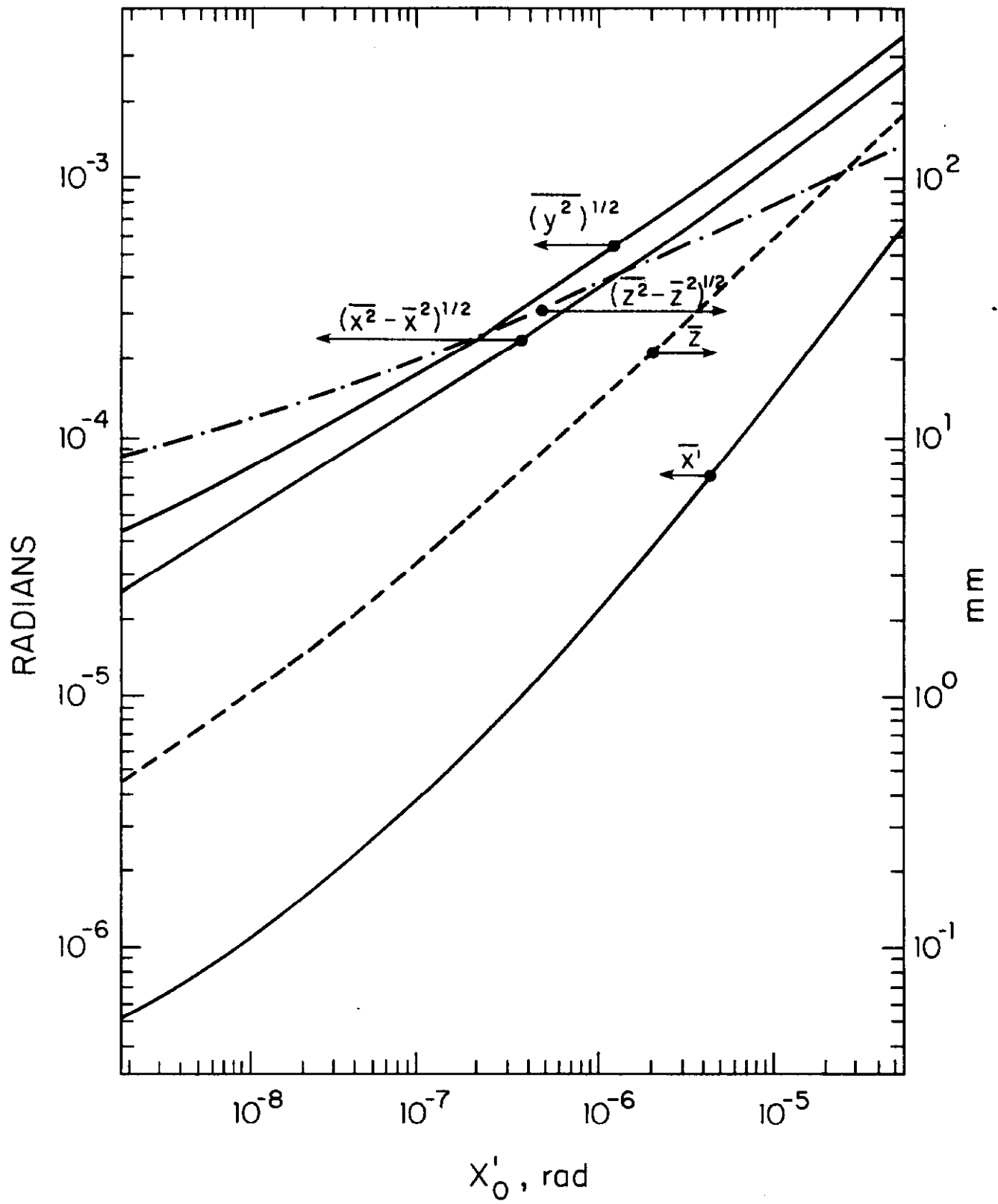


Fig. 19

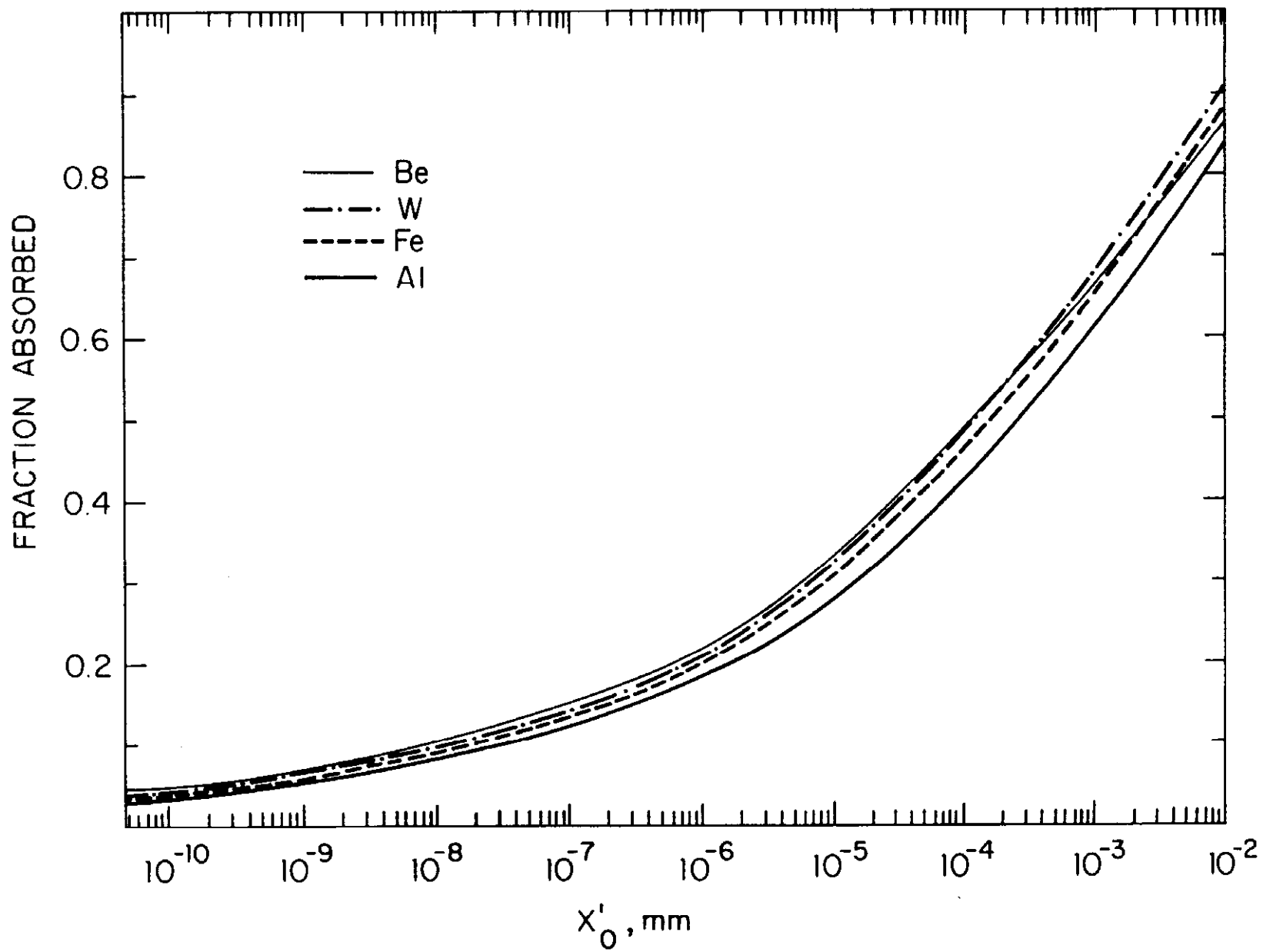


Fig. 20